VILNIAUS UNIVERSITETAS

CHEMIJOS IR GEOMOKSLŲ FAKULTETAS

CHEMIJOS INSTITUTAS

NEORGANINĖS CHEMIJOS KATEDRA

Abunaw Evelyn Enonchong

Pagrindinė studijų programa – Farmacinė chemija; magistro laipsnis

Baigiamasis darbas

Grafeno nanokompozitų, tinkamų elektrocheminių biojutiklių gamybai, ruošimas

Darbo vadovas: Prof. Jurgis Barkauskas

Konsultantas: Asist. dr. Justina Gaidukevic

Vilnius 2021

VILNIUS UNIVERSITY

FACULTY OF CHEMISTRY AND GEOSCIENCES

INSTITUTE OF CHEMISTRY/GEOSCIENCES

DEPARTMENT OF INORGANIC CHEMISTRY

Abunaw Evelyn Enonchong

Main study program – Pharmaceutical Chemistry; Master's Degree

Master's Thesis

Preparation of Graphene-based Nanocomposites with Enhanced Performance for Electrochemical Biosensors

Supervisor: Prof. Jurgis Barkauskas

Co-supervisor: Assisant Prof. Justina Gaidukevic

Vilnius 2021

TABLE OF CONTENTS

ACKNOWLEDGEMENT

Any piece of work like this is indebted to many people and this is not an exception. Words cannot adequately acknowledge the depth of my gratitude to all those who have contributed towards my success during this research project and studies in general. My special thanks and gratitude goes firstly to my supervisor Prof. Jurgis Barkauskas and co-supervisor Assistant Prof. Justina Gaidukevic for their expertise and guidance, and to Prof. Arunas Ramanavicius who has been of enormous help during my laboratory work with the assistance of Mr. Sarunas. A. Zukauskas to help me put down this piece of work. The entire Vilnius University and Pharmaceutical Chemistry department my appreciation to every one of you who ever said something positive to me to lead me through this road.

I also express my deep appreciation and recognition to my family my parents, for their love and support to help me pursue my dream, supporting me in every way possible. Furthermore, I would like to use this opportunity to express my appreciation to all my colleagues with whom we had the same spirit of sharing our knowledge and ideas. Last but not the least I would like to thank God Almighty most of all for making this entire work a success and putting a smile on my face because without God I wouldn't be able to do any of this.

LIST OF ABBREVIATIONS

GO	GO - Graphene oxide
NS-G	Graphene co-doped with nitrogen and sulphur
GOD	Glucose oxidase
DET	Direct electron transfer
SEM	Scanning electron microscopy
FTIR	Fourier Transform infrared spectroscopy
XPS	X-ray photoelectron spectroscopy
CNSs	Carbon nanostructures
CNTs	Carbon nanotubes
ORR	Oxygen reduction reaction
PBS	Phosphate-buffered solution
B. E.	Binding energy
N6	Piridinic N
N5	Pyrrolic N
NQ	Graphitic N
CV	Cyclic voltammetry

INTRODUCTION

After mechanical exfoliation of graphene monolayers by Andre Geim and Konstantin Novoselov by repelling graphite using the "adhesive tape" method in 2004, the area of nanocomposites sparked enormous interest that has prompted advancement in graphene-based materials for significant applications. Graphene and its derivatives are influential material on the horizon of material science, and are utilized in each and every field of research after their advent, [1]. Graphene oxide (GO) suspensions which is a derivative of graphene are amongst the most commonly used precursors to produce graphene-based nanocomposite materials. Graphene can be modified with organic molecules, polymers, or inorganic components in order to produced nanocomposites. Furthermore, graphene can be readily doped with heteroatoms like nitrogen, boron, phosphorus and sulphur due to its novel physical and electrochemical properties, which have drawn exceptional interest in the past years. Chemical doping of graphene with these heteroatoms leads to alterations in structural, electronic properties, and chemical reactivity of graphene as the size and electronegativity of the heteroatoms are different from those of carbon atoms. These alterations can successfully lead to modification in the properties of graphene material, such as thermal stability, charge transport, Fermi level, band-gap, localized electronic state, spin density, optical characteristics, and magnetic properties, [2]. Graphene derivatives doped with heteroatoms, like nitrogen and sulphur are highly promising materials for applications such as energy storage, fuel cells, sensing, electrocatalysis. Graphene co-doped with nitrogen and sulphur (NS-G) demonstrate great interest for their electrocatalytic activity due to the presence of extensive π-electrons in the structure. This enables this nanocomposite to exhibit superior oxygen reduction reaction and electrochemical sensing performances. The dual-doping of graphene with nitrogen and sulphur offers a synergic effects for the superior electrocatalytic properties. Glucose biosensors have received extensive attention over decades attributable to their extraordinary significance in biology, food industry, environmental protection and clinical analysis. Glucose oxidase (GOD) is the most basic catalyst for the development of enzyme-glucose biosensors in light of its low cost, bioactivity, and high sensitivity towards glucose detection, [3]. The challenge in the development of high-performance GOD-based glucose biosensors is to achieve the direct electron transfer (DET) process between the active sites of GOD and the surface of electrode. Chemical doping of graphene with heteroatoms like N, and S, can effectively modulate its electrical properties and enhance its electrocatalytic performances. This is due to the electrochemically active sites that are induced by doped heteroatoms, which are favorable for the adsorption and activation of analytes, anchoring of functional moieties or molecules, and accelerating the charge transfer between electrode and analytes/electrolyte, all of which would be advantageous to the enhanced electrochemical sensing performances, [4]

The purpose of this study was to synthesize a new electrocatalytically active graphene nanocomposite called nitrogen and sulphur co-doped three-dimensional graphene framework (NS-G), investigating its structure and evaluating this potential catalyst as a sensor for novel glucose oxidase (GOD) platform for the construction of GOD-based glucose. In order to achieve this goal, the following tasks were set:

- Synthesize GO by hummers method, followed by synthesis of nanocomposite NS-G by hydrothermal treatment.
- To evaluate the surface morphology by scanning electron microscopy (SEM)

- To assess the changes in the reaction mixtures and evaluate the formation of new chemical bonds in the NS-G nanocomposite by FTIR and to investigate the chemical nature of the NS-G nanocomposite by XPS.
- To study the structural changes of nitrogen and sulphur co-doped three-dimensional graphene framework (NS-G) at different compositions using raman spectroscopy.
- To analyze the electrocatalytic performance of NS-G nanocomposite as an electrochemical glucose biosensor.

In this study, NS-G was synthesized from hydrothermal treatment of GO and, water soluble ammonium thiocyanate (NH_4SCN) is chosen as N/S dual-containing precursor, which can form stable aqueous dispersion together with GO. A stable cross-linked GO hydrogel was induced using the pyrrole additive. The morphology, crystal and chemical structure of the prepared NS-G were characterized by FTIR, SEM, Raman spectroscopy and XPS and its electrochemical properties were examined in detailed.

1 LITERATURE REVIEW

1.1. Carbon nanostructures

Innovative nanomaterials with novel and unique properties are needed to maintain the current rate of advancement. Carbon nanostructures (CNSs) and their derivatives have received a lot of attention among nanomaterials, due to their unique properties and the potential for use in a wide range of existing and new applications. Carbon is an essential element on earth, which can be found in several structures in nature. It has been described as "the master element of living substances" [5]. Carbon atoms are described by their remarkable ability to form strong covalent bonds with other non-metals or with one another in a unique architecture to form extremely low-dimension structures like fullerenes, carbon nanotubes, graphene sheets and diamond-like carbon in various hybridization states, such as sp, sp^2, or sp^3, (Fig. 1.0.), resulting in a diverse variety of structures ranging from small molecules to long chains, [6, 7]. There is no other element like carbon that can form such diverse and completely different substances as a single element, in terms of structures and properties. In general, CNSs are recognized for their excellent electrical conductivity, supreme mechanical strength, high thermal conductivity, extraordinarily high surface area, excellent photo-luminescent properties, high transparency and structural stability. These unique properties make carbon nano-architectures promising for applications stretching from thin film transistors, transparent conducting electrodes, photovoltaics, supercapacitors, to biosensors, drug delivery, tissue engineering, and photothermal therapy, [7].

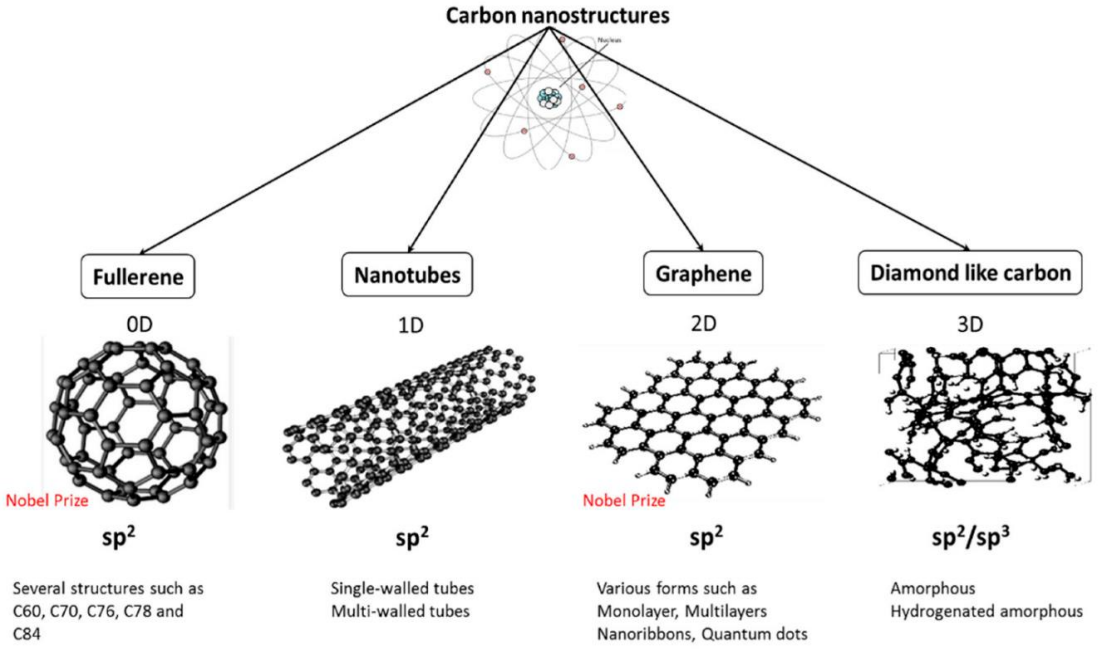

Fig. 1.0. Several forms of carbon nanostructures.

There are numerous ways that carbon nanomaterials could be classified, amongst include synthetic conditions, physical properties, and types of covalent bond, morphological characteristics and their dimension, [8]. On the basis of the predominant type of covalent bond, carbon nanomaterials can be divided into two categories namely; the graphene-like nanostructures, which are primarily made up of sp^2 carbon atoms that are densely packed in a hexagonal honeycomb crystal lattice. However, they may

also contain some sp^3 carbon atoms at the edges or defect sites. This group includes graphene, carbon nanotubes (CNTs), nanohorns, onion-like carbon nanospheres, and carbon dots; the second category of carbon nanomaterial contain both sp^3 and sp^2 carbon atoms in various ratios and have mixtures of amorphous and graphitic regions, or consist mainly of sp^3 carbon atoms. Nano-diamond and carbon dots with non-graphitic structures are the only known members of this group, [9]. Moreover, on classification based on dimensionality, carbon nanomaterials could be 0D (fullerenes, OLC structures, carbon dots), 1D (CNTs, carbon nanofibers, and SWNHs), 2D (graphene, graphene nanoribbons) or 3D (diamond, graphite) dimension structures, [9]. Two-dimensional (2D) nanomaterials have gained a worldwide attention in recent years because of their outstanding properties. The 2D nanomaterials offer promising opportunities for various applications to be used in an exfoliated state, as single- or few-layer structures, at scientific and technological levels. The most widely known 2D layered material is graphene, [9 - 10].

Carbon exist in different allotropes with the most usual and stable ones being graphite and diamond. Graphite consists of a layered structure made of hexagonal rings of carbon atoms with sp^2-hybridization. These layers are linked by Van der Waals forces that generate an exfoliating structure. Due to the weak forces between the graphite layers, it is possible to isolate one of these layers to obtain graphene (G), an atomically thick two-dimensional sheet comprising sp^2 carbon atoms tightly packed into a honeycomb crystal lattice with bond length of about 0.141 nm, [11-12].

1.2. Graphene

Graphene being a monolayer made up of carbon atoms belongs to the two-dimensional (2D) ultrathin nanomaterials family. It is the basic structural element of some carbon allotropes and can be considered as mother of all graphitic forms, [13], or the "building block" of the other graphenic/ graphitic nanoallotropes. This is because, a properly cut piece of a graphene sheet could in principle be wrapped up to form the 0D fullerene, rolled up to form a 1D CNT, or stacked with additional sheets of graphene to form multilayered stacked into 3D graphite. As demonstrated in Fig 1.1, more complex graphenic nanostructures such as nanohorns can conceptually be obtained by elaborating on the structure of graphene in more sophisticated ways, [9].

.

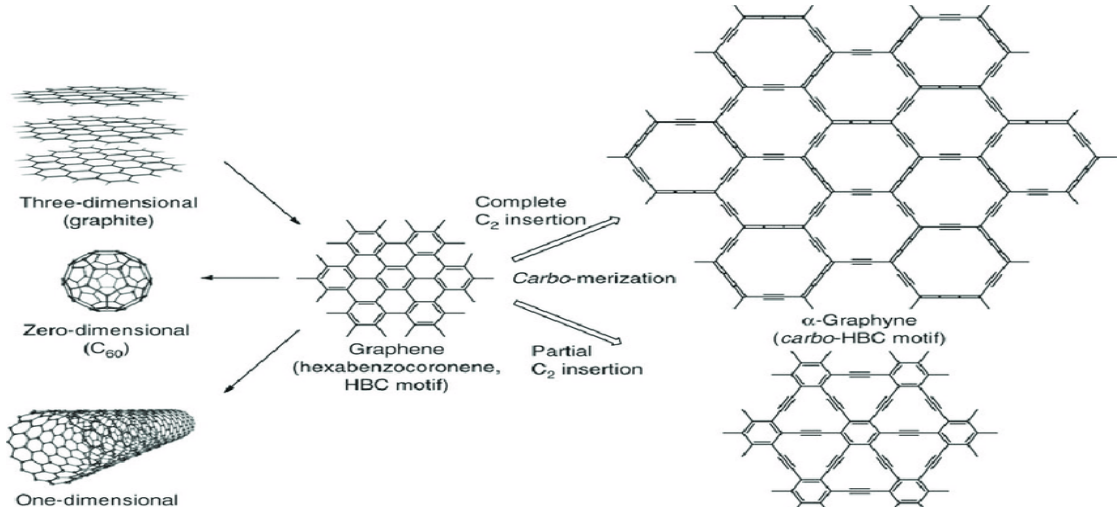

Fig. 1.1 Chemical structure of graphene material, [15].

1.2.1 Chemical and physical properties of graphene

Micro mechanical exfoliation of graphite crystals was used to create this one-atom-thick nanostructure by Andre Geim and Konstantin Novoselov in 2004, which was accompanied by a series of methods such as exfoliation by graphite oxides or graphite intercalation compounds, chemical vapor deposition, etc. Graphene rapidly rises to be a spotlight on the materials horizon due to its extraordinary physical, chemical, and mechanical properties with values that surpass those obtained in any other materials. For instance: high specific surface area (2640 $m^2 g^{-1}$), very high electron mobility (25,000 $cm^2 V^{-1} s^{-1}$), thermal conductivity (3000-5000 $W \cdot m^{-1} \cdot K^{-1}$) which is superior to that of copper (around 400 $W \cdot m^{-1} \cdot K^{-1}$) and, the highest electrical conductivity known at room temperature (~6000 S cm^{-1}) with mobility of ~200,000 cm^2 V s^{-1}, mechanical strength, antimicrobial activity, and it is impermeable to gases, [11-12, 14]. Furthermore, graphene is a zero-band gap semiconductor material, where the charge carriers have a linear dispersion relationship near the Dirac point, essentially giving them zero effective mass, it is electroactive and transparent, absorbing only 2.3% of the incident light and presents a high Young's modulus and Poisson's are 1.02 TPa and 0.149, respectively and an ultimate strength of 130 GPa, thus being the strongest material ever measured, stiffer than steel. These unique properties make graphene an ideal candidate for a wide range of applications such as sensors, supercapacitors, fuel cells, photovoltaic devices, batteries, nanocomposites, and flexible electronic devices. [11-12, 15]. Graphene is aromatic in nature possessing highly dense electron cloud which are both above and below the plane. Frontier molecular orbitals of organic molecules can easily interact with the π-electrons of graphene making electrophilic substitution of graphene much easier than nucleophilic substitution, [16]. Graphene can take part in certain classes of reactions including cyclo-additions, click reactions, and carbene insertion reactions. However, reactions on the surfaces of graphene has a restraining influence to its planar structure and this causes destruction of the sp^2 structure leading to the formation of defects and loss of electrical conductivity, [16]. The chemical reactivity of geometrically strained regions of graphene lattices is much higher in comparison with other regions. This is attributed to the easier displacement of electron density above the plane of the ring, [17]. Furthermore, the 2D nature of graphene sheets, enables the edge regions to play an important role in the electronic structure of the molecules. The edges can manifest as either zig-zag tracks or arm-chair tracks. It was found that, the zig-zag edges of graphene display higher chemical reactivity compared to arm-chair edges, this is because in the zig-zag edges, the attainment of aromatic sextets is perturbed in the majority of the rings, hence such a structure is thermodynamically unstable compared to the arm-chair edges. It can be expected that the zig-zag edges will display higher reactivity as compared to the arm-chair edges, [16, 18].

1.2.2 Derivatives of graphene

GO a derivative of graphene has been used widely as a starting material for the synthesis of graphene-based nanocomposites. The surfaces of GO sheets contains highly oxygen bearing groups like; hydroxyl, epoxide, diol, ketone, and carboxyl functional groups (Fig. 1.2.), that can alter the van der Waals interactions significantly and are responsible for the hydrophilic properties and dispersibility of GO in water or other polar organic solvents, allowing the graphene sheets to inculcate different types of nanoparticles or nanocluster, [19, 20]. The hydroxyl and epoxy groups which are bonded to sp^3

hybridized carbon on the basal plane, in addition to quinone, lactone, carbonyl and carboxyl groups located at the edges of sp^2 hybridized carbon, [21]

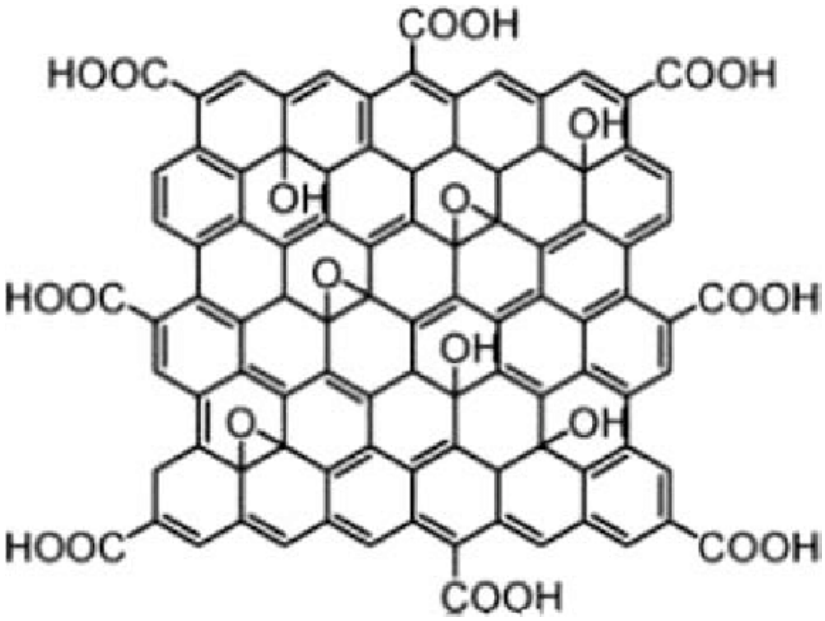

Fig. 1.2. Illustration of GO Structure showing presence of oxygenated groups.

However, the reduction of GO dispersion without stabilizer leads to precipitation of graphite particles due to the rapid, irreversible agglomeration of single layer graphene sheets. Therefore, prior to reduction, surface modification of GO sheets is usually carried out by covalent modifications or non-covalent functionalization, followed by reduction. GO suspensions are among the most commonly used precursors to produce graphene coatings and graphene-based nanocomposite materials. Graphene can be modified with organic molecules, polymers, or inorganic components in order to produced nanocomposites.

Water soluble ammonium thiocyanate (NH_4SCN) can be used as Nitrogen/Sulphur dual-containing precursor, which can form stable aqueous dispersion together with GO for the synthesis of graphene nanocomposite called nitrogen and sulphur co-doped three-dimensional graphene framework, whereby the thiocyanate fragments undergo polymerization, [22]. Hydrothermal treatment NH_4SCN at 443 K, it undergoes the decomposition into highly reactive N/S-rich species, such as NH_3, H_2S, CS_2 etc. which can react with the defective sites and oxygen-containing groups of GO. Simultaneously, GO can be reduced to graphene and assemble into 3D graphene fragments during the hydrothermal process, [23]. Stable cross-linked GO hydrogel can be induced using pyrrole, [22]. Pyrrole function not only as a cross-linker but also as the heteroatom-containing polymer dopant precursor to realize uniformly distributed and high level multiple dopant. Furthermore, pyrrole functions as a pore-creating agent to create the 3D hierarchical porous structure, which plays an essential role in the successful synthesis of the NS-G, [22].

1.3. Chemical functionalization of graphene

Functionalization refers to the addition of functional groups to a compound by chemical synthesis. The applications of pristine graphene have been restricted to a great extent, due to the absence of an intrinsic band-gap, in the field of nanoelectronics, sensing, electrocatalysis and energy storage. It is

therefore attractive to encourage a band gap in graphene to promote the above-mentioned applications, [23, 24]. Graphene is characterized as a zero band gap semiconductor or semimetal because its density of states is zero at the Fermi energy level, [9]. Hence, functionalization and dispersion of graphene sheets are of crucial importance in their applications. So the absence of a band-gap in graphene constitutes one of the fundamental problems that needs to be resolved before the material can be deployed in most applications. A few strategies have been proposed to open the electronic band gap in graphene, like molecular adsorption, confinement, chemical functionalization, multilayer graphene and edge-effects-induced band-gap, [25]. The chemical functionalization of graphene offers an alternative approach to the control of its electronic properties. GO chemistry provides a scalable, low-cost approach to obtaining a functionalized graphene than pristine graphene and rGO. By careful and controllable modification of the specific oxygenated functional groups, the electrical, optical, and/or chemical properties of graphene materials can easily be tailored. Chemical functionalization could be obtained by covalent modifications or non-covalent functionalization.

1.3.1. Covalent modification

Generally, there are two routes for the covalent functionalization reactions of graphene: the formation of covalent bonds between free radicals or dienophiles and C=C bonds of pristine graphene; and the formation of covalent bonds between organic functional groups and the oxygenated functional groups of GO or rGO, [26]. These modifications either take place at the end of the sheets and/or on the surface, for instance carboxyl groups at the periphery, and epoxy, hydroxyl, and –C = C– groups in the basal plane, [27]. Surface functionalization involves rehybridization of one or more sp^2 carbon atoms of the carbon network into the sp^3 configuration accompanied by simultaneous loss of electronic conjugation and this can be achieved in four different ways: nucleophilic substitution, electrophilic addition, condensation, and addition, [28]. Modification of graphene with amine ($-NH_2$) group is by condensation and nucleophilic substitution of the carbonyl or epoxy of GO with $-NH_2$ functionality of the organic modifiers bearing a lone pair of electrons which attacks the these oxygenated groups of the GO at room temperature, [29]. Electrophilic substitution reactions with graphene involve the displacement of a hydrogen atom by an electrophile. Spontaneous grafting of aryl diazonium salt to the surface of graphene is an example of electrophilic substitution, [30].

1.3.2. Non-covalent functionalization

Non-covalent functionalization is a well-known technique for the surface modification of carbon-based nano-materials. This technique has been previously employed extensively in the surface modification of the sp^2 networks of carbon-nanotubes, [31]. Unlike covalent functionalization, non-covalent functionalization is based on the π-π interaction, hydrophobic attraction, or van der Waals force between graphene materials (GM) and stabilizers not only cause less negative impact on the structure of graphene materials, but, also provides the feasibility to tune their solubility and electronic properties, and requires the physical adsorption of suitable molecules on the graphene surface, [27]. Non-covalent functionalization is achieved by polymer wrapping, adsorption of surfactants or small aromatic molecules, and interaction with porphyrins or biomolecules such as deoxyribonucleic acid (DNA) and peptides, [32].

1.3.3. Chemical activity of graphene surface

As earlier mentioned, chemical functionalization of graphene offers an alternative approach to the control of its electronic properties for technological applications. Many functionalization methods such as chemical bonding, functional groups and free radicals on graphene have been utilized to improve the surface activity of graphene, which will render it with more novel properties through modifying the chemical, structural and electronic properties of graphene. One simple and effective method is to adsorb H or F atoms on graphene, which changes the hybridization of C atoms from sp^2 into sp^3 to open the band gap of graphene, hence change in its electronic structure resulting to conversion from a metallic graphene to an insulator, [33]. It has been reported from previous studies on the layer dependent chemical activity of n-layer graphene on SiO_2/Si substrate. In this study, the Raman spectrum indicated that monolayer graphene was much more feasible to being fluorinated and hydrogenated than multilayer graphene, which was attributed to the lack of π-stacking due to the out-of-plane deformation caused by the substrate, [34]. Pristine which is considered as ideal graphene contains only a single layer of carbon atom with sp^2 hybridization whereas reduced graphene obtained from the reduction of GO still has tiny oxygen-containing groups on its surface. The presence of this functional groups brings about change in the structure of graphene, hence influences the properties of graphene, [35]. Although the pristine graphene has the highest theoretical strength, its perfect honeycomb lattice makes graphene chemically inert. However, the presence of functional groups on graphene surface can modify its surface chemistry, and benefits dispersibility in some solvents and matrixes, [35].

The property of graphene-polymer composite is mainly determined by the synergic combination of high specific surface area of graphene, strong filler-matrix interfacial adhesion, the exceptional properties of graphene, and as well as by the essential properties of the matrix. The interfacial adhesion is determined by matrix properties and surface properties of graphene, such as the total surface area of graphene available for contact with matrix molecules; surface roughness of graphene, which may allow for mechanical interlocking; the chemical structure and surface energy of graphene, which determine whether the graphene will be wetted by the matrix, as well as by the surface functional groups for forming attractive interactions, in particular, chemical bonds with matrices or polar interactions (such as Lewis acid-base interactions and hydrogen bonds) with matrices, [36]. Therefore, the surface properties of graphene and surface/ interfacial interaction between graphene and matrix play crucial roles in control of the properties of composites. Furthermore, surface properties are especially important for hybrid materials and coatings which are used in biomedical, electronic and energy applications, [37].

1.3.4. Doping

The motivation of doping is to control the type and concentration of charged carriers. Amongst the few strategies purposed to open the electronic band-gap, chemical doping which is one of the approaches to recondition the electronic, chemical, and magnetic properties of materials is a powerful strategy to modify electronic properties, control surface science and alter the natural structure of materials. [2, 16]. For carbon materials, chemical doping is also a leading potential strategy to enrich free charge-carrier densities and enhance the electrical or thermal conductivities, [38]. Chemical doping, is usually of two types namely; surface transfer doping, which involves the adsorption of foreign agents onto the surface

of graphene which do not cause sp^3 defects in the graphene cross-section; substitutional doping, involves the disruption of the sp^2 network by foreign agents which create sp^3 defect regions through covalent bonding with graphene. Graphene can be p-type or n-type doped via chemical doping. p-type doping drives the Dirac points of graphene above the Fermi level, and n-type doping drives the Dirac points below the Fermi level. Molecules with electron withdrawing groups adsorbed on the surface of graphene will lead to p-type doping of graphene, and molecules with donating groups like nitrogen will lead to n-type doping, [39]

Graphene can be doped with heteroatoms like nitrogen and sulphur, causing structural and electronic alterations, hence modifications in the properties of graphene material. Chemical doping of graphene with heteroatom can significantly modify its active sites, modulate its electrical properties and enhance its electrocatalytic performances, [40-41]. Among the numerous potential dopants, nitrogen (N) is considered to be an excellent element for the chemical doping of carbon materials because it is of comparable atomic size and contains five valence electrons available to form strong valence bonds with carbon atom, [38]. The electronic structure (such as charge density) of carbon-based materials can be tuned by doping nitrogen into the sp^2 -hybridized carbon skeleton, because the electronegativity of nitrogen (3.04) is higher than that of carbon (2.55), consequently creating charged sites to facilitate the adsorption and reduction of oxygen molecules, [22]. Doping of CNTs with nitrogen has been shown to modify its electrical and structural properties by increasing the metallic behavior, affecting the lattice alignment and enhancing the biocompatibility and sensitivity in biosensing applications. N doping has great potential to be used for graphene modification, [38]. The incorporation of nitrogen in graphene-based materials enhances the charge carrier density due to the involvement of p-electrons of nitrogen with the p-system of graphene. Hence, nitrogen and groups based on it play a significant part in the electrochemical study of N-doped materials. Some experimental studies have revealed that dual-doping of N with other elements, such as S, B or P further increases the electrochemical properties due to the synergistic effect arising from the coupling interactions between two heteroatoms, [41]. Graphene co-doped with nitrogen and sulphur (NS-G) demonstrate great interest for their electrocatalytic activity due to the presence of extensive π-electrons in the structure. This enables this nanocomposite to exhibit superior oxygen reduction reaction and electrochemical sensing performances. The dual-doping of graphene with nitrogen and sulphur offers a synergic effects for the superior electrocatalytic properties. The nitrogen group is capable of transforming two-electron transfer to four-electron transfer on the doped carbon materials, and the sulfur-group is beneficial to optimize onset and half-wave potentials. Therefore, nitrogen and sulfur-codoped carbon materials have shown extraordinary oxygen reduction reaction (ORR) performance, [22]

1.4. Electrochemical biosensors

Electrochemical biosensors are based on measuring biological binding event-dependent changes in conductance, resistance, or capacitance of the biosensor surface. In these devices, one of the electrodes is immobilized with a biological recognition molecule. Analyte binding to biological recognition element triggers a change in electrical properties due to oxidation and reduction reactions taking place as a result of biological interaction activity, thus providing the sensor signal, [42]. Electrochemical biosensors rely mostly on enzyme-catalyzed reactions to produce current/potential difference which is then detected, example is Glucose biosensors, [43]. Over the past decades, there has been a lot of interest on glucose

biosensors due to their great importance in biology, food industry, environmental protection and clinical analysis. Glucose oxidase (GOD) is the commonest enzyme for the construction of enzyme glucose biosensors because of its low cost, bioactivity, and high sensitivity towards glucose detection, [41]. The major challenge in the development of high-performance GOD-based glucose biosensors is to achieve the direct electron transfer (DET) process between the active sites of GOD and the surface of electrode because the electroactive center of GOD, flavin adenine dinucleotide (FAD), is deeply buried inside the GOD shells, rendering them inaccessible for DET with bare electrodes. In order to overcome this problem, graphene, and their composites have been used to modify the electrode to immobilize GOD for improving the DET between GOD and electrode. [41].

Surface electrochemical active sites and charge transfer are the two key properties that directly determine the performance of electrochemical sensors, [40].The electrochemically active sites induced by doped heteroatoms are favourable for the adsorption and activation of analytes, anchoring of functional moieties or molecules, and accelerating the charge transfer between electrode and analyte/ electrolyte, all of which would favour an enhanced electrochemical sensing performance, [2, 41]. Due to the presence of extensive p-electrons in the structure of graphene and graphene-doped materials, they are of interest for their electrocatalytic activity, [2]. It has been reported that co-doping graphene provides a more powerful electrocatalytic activity for oxygen reduction reaction (ORR) compared to those of single N-doped graphene (N-G). The performance of electrochemical sensors can also be notably improved by the use of co-doped graphene materials, [44]. On the basis of the advantages of dual heteroatoms doping and encouraging reports, it is anticipated that the co-doped graphene may well modify the electrode for improving the direct electron transfer (DET) of GOD on the surface of electrode, which can be used for electrochemical detection of glucose. [41].

2 EXPERIMENTAL

2.1 Materials and reagents

All reagents and materials were of analytical grade or high purity, and unless otherwise stated were used as received. Graphite used for the synthesis was of extra pure grade (Merck). The particle size of the pristine graphite (according to manufacturer's data) was ≥50.0 μm (99.5 %). Graphite rod was used for the preparation of working electrodes. Deionised water was used for solutions preparation and washing. Sulphuric acid (H_2SO_4), sodium nitrate ($NaNO_3$), hydrochloric acid (HCl), potassium permanganate ($KMnO_4$), hydrogen peroxide (H_2O_2), ammonium thiocyanate (NH_4SCN), pyrrole, Nadir® - dialysis tubing cellulose hydrate (Carl Roth), polycarbonate membrane filter, phosphate-buffered solution (PBS), glucose oxidase.

2.2 Sample preparation

2.2.1. Synthesis of graphene oxide

3 g of sodium nitrate was added to cold (3 °C) 240 mL of concentrated sulphuric acid, while stirring the temperature was maintained 5 - 6 °C. 6 g of graphite powder was gradually added to the mixture. 30 g of potassium permanganate ($KMnO_4$), was added in portion under stirring and the temperature of the mixture was maintained between 5 - 6 °C by cooling with water bath. The resulting mixture was left at room temperature for 7 days. Successively the mixture was heated at 35 °C for 1 hr under continuous stirring, and then carefully diluted with 276 mL of deionized water. The addition of water causes a rise in temperature of the mixture, hence temperature was maintained between 60 – 70 °C for 1 hr.

Fig. 2.0 Synthesis of graphene oxide.

Thereafter additional 840 mL of deionized water was then added. Shortly, 25 mL of 30 % H_2O_2 was added to the mixture while stirring resulting to brilliant-yellow colour mixture of GO which was then filtered and washed with 10 wt% HCl (1.0 L) aqueous solution to remove metal ions as seen in Fig. 2.1. Afterwards, the filtered cake of GO was transferred into a dialysis tubing cellulose membrane with a cutoff molecular weight (MWCO) of 10000 – 20000 Da and dialyzed against distilled water until the dialysate was free of sulphate ions and exhibited a pH of 6. The suspension was filtered using a Buchner funnel and obtained brown powder was dried in a vacuum desiccator to a constant weight.

2.2.2. Synthesis of nitrogen/sulphur co-doped 3D graphene framework (NS-G)

0.5 g of GO was mixed with 3 mL of deionized water. 13.2 uL of pyrrole was added to the GO suspension followed by the addition of 12.5 mL of NH_4SCN, and the suspension was made to the mark of 50 mL, mixed and sonicated for 1 hr. the suspension was then transferred to a Teflon line stainless steel autoclave, and heated in a muffle oven at a temperature of 180 °C for 10 hrs, after which it was allowed to cool down to room temperature. The resulting hydrothermal monolith sponge-like sample, (Fig. 2.1) was washed and filtered with excess water followed by drying for 2 days, to yield a low density carbonaceous aerogel. The sample stored in the refrigerator until further analysis. The resulting materials are denoted as N/S-G as shown on Table 1 for the different content of NH_4SCN, and pyrrole respectively. The control samples was prepared under the same conditions.

Fig. 2.1. Sponge-like NS-G prepared by hydrothermal analysis

Table 1. Mass and volume of GO and precursor materials, indicating their ratio and nanocomposites.

Precursors	Volume (µL) and mass (g)	Ratio	N/S-G nanocomposite
NH_4SCN + GO	0.0125 g (12500 mL) + 0.5 g	1:40	N/S-G 1:40
Pyrrole + NH_4SCN + GO	0.0125 g (13.2 µL) + 0.0125 g (12.5 mL) + 0.5 g	1:1:40	N/S-G 1:1:40
Pyrrole + NH_4SCN + GO	0.25 g (263.8 µL) + 0.0125 g (12.5 mL) + 0.5 g	20:1:40	N/S-G 20:1:40
Pyrrole + NH_4SCN + GO	0.5 g (527.6 µL) + 0.0125 g (12.5 mL) + 0.5 g	40:1:40	N/S-G 40:1:40
GO control	0.5 g		GO

2.3. Sample characterization

2.3.1. Fourier Transform infrared spectroscopy (FTIR)

Measurements of FTIR were done using a Frontier (PerkinElmer) FTIR spectrometer in the range 600 – 4000 cm^{-1}. Samples preparation were done by utilizing KBr pellet technique. Sample powder (0.5 percent by weight) was mixed with pure KBr powder for this reason. Sample powder (0.5% by wt) was

mixed with pure KBr powder for this reason. By utilizing a PIKE CrushIR hydraulic press with an 8 ton • cm^{-2} pressure, the mixtures were pressed into transparent pellets for 5 minutes. A reference blank KBr pellet was used for background corrections. All spectra were acquired from 100 scans with the spectral resolution of FTIR spectroscopes set at 4 cm^{-1}.

2.3.2 X-ray photoelectron microscopy (XPS)

Monochromatic Al K radiation was used to conduct X-ray photoelectron spectroscopy analyses in a Kratos Axis Supra spectrometer (1486.69 eV). The base C 1s peak at 284.6 eV was used to calibrate the binding energies. The raw XPS spectra were deconvoluted using the software CASAXPS and curve fitting peak components. After Shirley-type background subtraction, symmetric Gaussian–Lorentzian product functions were used to approximate the line shapes of the fitting components. Experimental intensity ratios were used to measure atomic ratios, which were then normalized using atomic sensitivity variables.

2.3.3 Scanning electron microscopy (SEM)

Scanning electron microscope images were taken using a Hitachi SU-70 microscope at an accelerating voltage of 5.0 kV at various magnifications.

2.3.4 Raman spectroscopy

Raman spectra were recorded using an inVia Raman spectrometer (Renishaw, Gloucestershire, UK) equipped with a thermoelectrically cooled (−70°C) CCD camera. The He-Ne gas laser was provided an excitation beam at 532 nm with power restricted to 1mW. The integration time was 100 s.

2.4. Electrochemical measurements

Electrochemical measurements of NS-G nanocomposite 40:1:40 were performed using an electrochemical system "μSTAT 4000" with a conventional three-electrode system made of a Ag/AgCl (KCl, 3 M) reference electrode, a platinum plate counter electrode, and a working electrode of graphite rod (Ø 3 mm) coated with NS-G nanocomposite and glucose oxidase (GOD) as shown in Fig. 2.2. The working electrode preparation was done by polishing the graphite rod with thin abrasive paper then wash with deionized water and air dried. Thereafter, 4.1 mg of NS-G 40:1:40 was dispersed in 4.1 mL of isopropanol and then sonicated for 30 minutes. 5 uL of the dispersed suspension was then deposited on the electrode surface and allowed to air dry at room temperature. Then, 2.5 μL of GOD (5 mg/mL) was then immobilized on the electrode and dried again. The electrode was then suspended in glutaaldehyde (linker) for 15 minutes, thereafter rinse with deionized water and the electrochemical cell was then set up. For control experiment, the same procedure was done for GO.

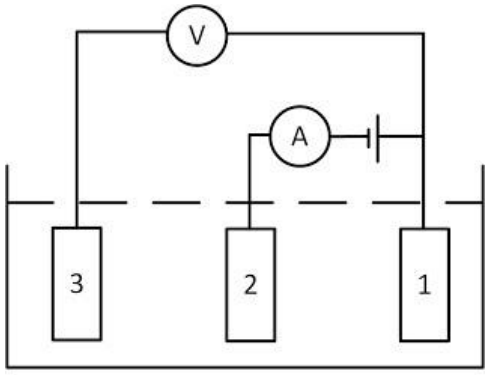

Fig. 2.1. Schematic illustration of conventional three-electrode system 1. Working electrode. 2. Counter electrode. 3. Reference electrode

The electrocatalytic activity of prepared electrode towards biosensing was examined using a cyclic voltammetry (CV) and chronoamperometry. The CV measurements were conducted by sweeping the potential from -0.8 V to 1 V in 20 mL of phosphate-buffered saline (PBS) + 0.1 M KCl (pH 7) with a scan rate (5 mV/s) in the presence and absence of 0.1 M glucose. Chronoamperometry measurements were carried out at a potential of 600 mV with the addition of 0.1 M glucose at different volumes: 100 µL *6; 200 µL * 2; 300 µL * 2; 500 µL * 2. All measurements were carried out at ambient temperature of 22 °C.

3 RESULTS AND DISCUSSION

3.1. Physico-chemical characterization of the nanocomposite

3.1.1. SEM analysis

SEM images reveal characteristic platelet structure of GO, (Fig. 3.1A). The SEM images of GO and rGO (Fig. 3.1B) reveal that the synthesized samples are in the form of flakes of few micrometer in size. The wrinkles on the structure of GO & rGO can be easily seen from the SEM images. It has been reported that the wrinkles in the structure of graphene sheets enhances its charge accumulation capability.

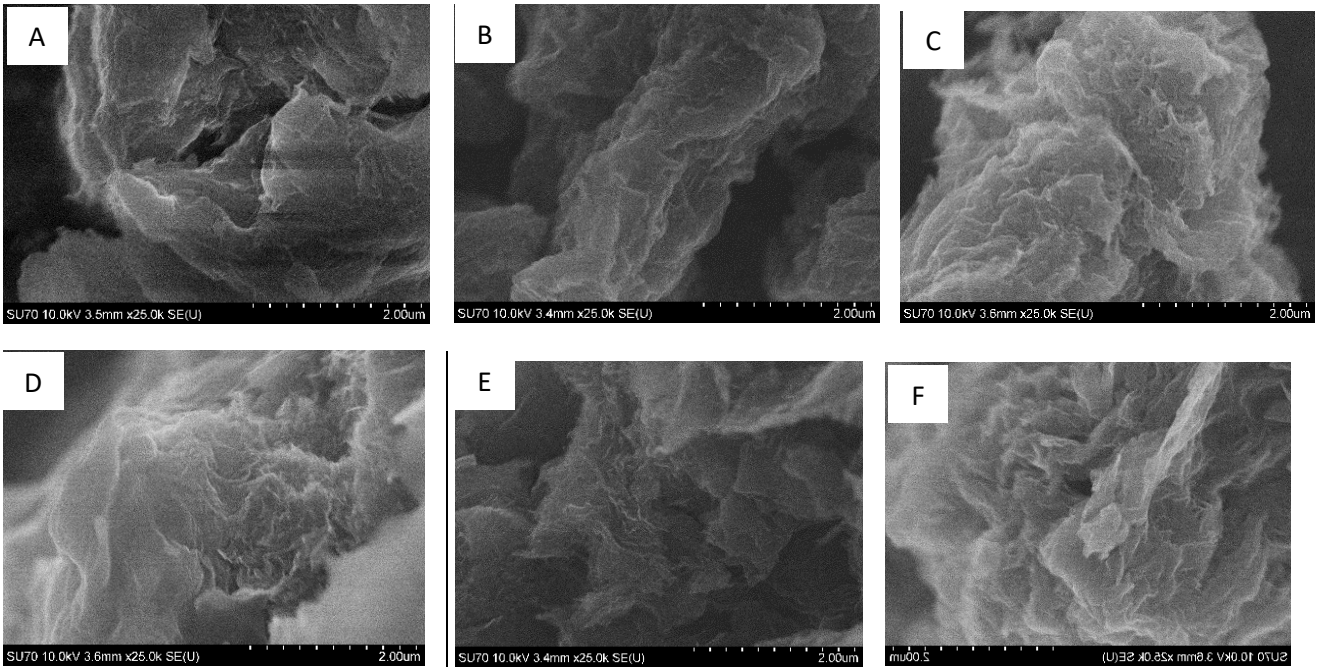

Fig. 3.1 SEM images showing change in morphology from GO to nanocomposites. A) GO, B) rGO, C) NS-G 1:40, D) NS-G 1:1:40, E) NS-G 20:1:40, F) NS-G 40:1:40

During modification, N/S-G nanocomposites exhibited a fluffy, distinct, crumpled, and highly rough and porous 3-D network of curled structure. The higher the concentration of pyrrole, the more curled the material, (Fig. 3.1 D, E, F). The curled, rough morphology might have originated from defective structures formed during heteroatoms doping process which occurs on the edges of GO sheets leading to a formation of free-stacking of the wrinkles on the edges of GO platelets. [45-47]

3.1.2. FTIR spectra analysis

FTIR spectra analysis was performed to investigate the structure and functional groups of the nanocomposites (Fig. 3.2). Below illustrates the changes occurring in the FTIR spectrum of GO upon hydrothermal treatment with NH_4SCN and pyrrole. The most characteristic features in the FTIR spectrum of GO are the adsorption bands corresponding to the C=O carbonyl stretching of carboxylic group (COOH) at 1731 cm^{-1} , adsorption at 1401 cm^{-1} indicating O–H deformation vibration of tertiary C-OH. The C–OH stretching vibration of phenol at 1221 cm^{-1}, and the C– O stretching vibration of epoxy group

at 1077 cm^{-1}. Other than the common O–H stretches which appear at 3405 cm^{-1} as a broad and intense signal, the peak at 1626 cm^{-1} can be assigned to C=O stretching mode of quinone group but may also be related to vibrations of the adsorbed water molecules, [48-51].

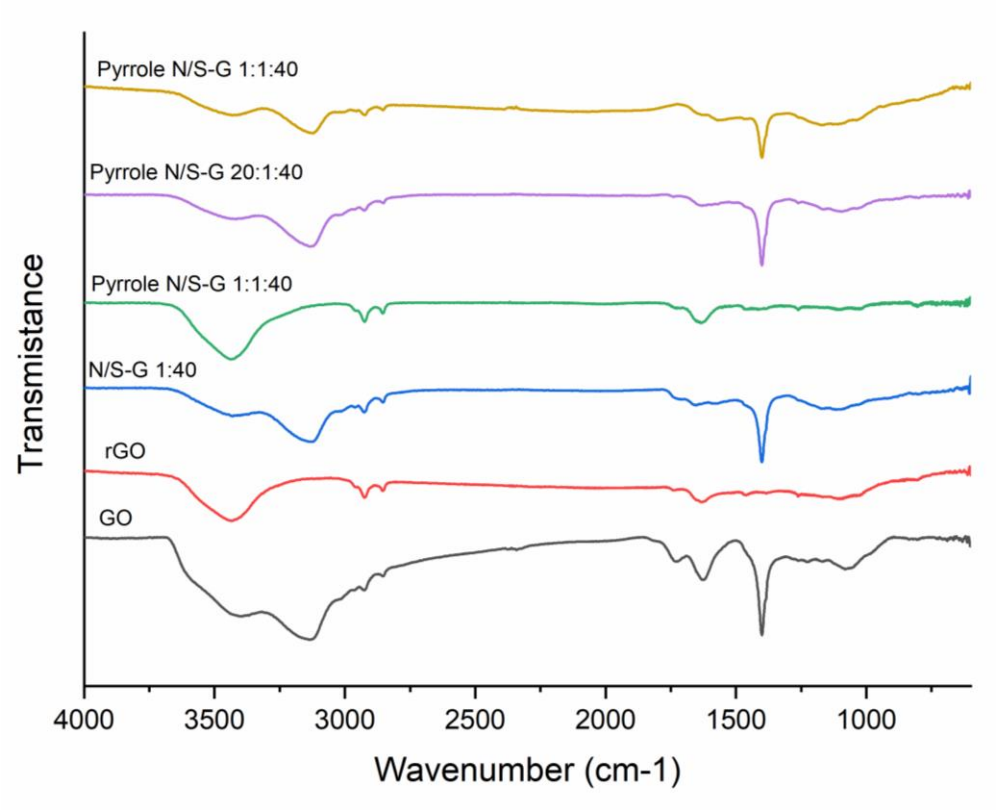

Fig 3.2 FTIR spectra of GO, rGO and NS-G nanocomposites.

Upon modification with NH_4SCN and pyrrole, some peaks disappear or decrease in intensity, while other peaks appear. Thus, in the region 1077 cm^{-1} the peak of epoxy group in GO disappears, and upon modification, appears a new peak at ~1120 cm^{-1}. This new peak indicates the existence of C-N and or C-S vibrations. Similarly, the peaks at 1626 cm^{-1} (quinone) disappears and a new peak is seen at 1557 cm^{-1}. The source of this new band could be amides, corresponding to the coupling of C-N stretching vibrations with –HC=N deformation vibration called Amide II vibration. Furthermore, the peak at 1731 cm^{-1} (-C=O in carboxyl-group) disappear, and new peaks appear at 1633 cm^{-1} due to amide carbonyl-stretching mode called Amide I vibrational stretch. All these newly appeared peaks can be attributed to the vibrations in –C=N- conjugated group. The vibration of C=N in the absorption area indicates the occurrence of C double bonds on GO with N dopants from NH_4SCN and pyrrole. Whereas the C-N and or C-S vibrations indicates a C single bond on GO with N and or S dopants from NH_4SCN and pyrrole. The appearance of the peak at 1557 cm^{-1} overlaps with C=C thus can also be assigned to the presence of C=C stretching in extended conjugated bonds. The FTIR spectra confirm the presence of C=N, CN, and C-S bonds indicating that the doping of nitrogen and sulphur atoms has successfully entered the GO structure. Similar results were reported by [48, 52].

3.1.3. XPS analysis

XPS was used to investigate the surface chemistry of the N/S-G. The XPS survey scan displayed the C, O, N, and S peaks without any noticeable impurities. The XPS measurements showed that all the SN-G contained nitrogen and sulphur as expected from the choice of precursor materials (NH_4SCN). On the basis of elemental analysis (Table 2), the presence of N (0.548963 %) and S (1.04484 %) elements in the GO material is assigned to the use of sodium nitrate and sulfuric acid respectively during GO preparation and related groups nitrates (NO_3) and sulphates (SO_4) which can be retained at the surface. After undergoing, hydrothermal treatment with NH_4SCN, the mass % of N and S decrease (0.272711 % and 0.194368 % respectively). This can be explained by the fact that the functional groups NO_3 and SO_4 introduced during GO preparation has been leached out from the surface during the aqueous solution reaction and washing procedures, hence XPS is a surface analysis technique covering 10 nm deep from the surface. However new functional groups of N and S are introduced during the hydrothermal treatment with NH_4SCN, explaining the resulting N and S seen in the nanocomposites. Furthermore, there is increase in the atomic percentage of both N and S upon the use of pyrrole. It was seen that increasing the amount of pyrrole rapidly increased the amount of these heteroatoms incorporated into the graphene sheet as seen on Table 2. This justifies that pyrrole acts as a cross-linker to retained these heteroatoms into the graphene framework and also as an N-precursor. Doping and reduction process consumes the oxygen-containing groups and leading to the deoxygenation of GO. This is evident in Table 2 as the O content of the various nanocomposites and rGO decrease significantly compared to that of GO (29.0068 at. %), as the atomic percentages of N and S increase for the former. This results are similar to that observed by G. Chen et al [41].

Table 2. Elemental analysis expressed in atomic percentages for GO, rGO and all NS-G nanocomposites.

Sample	Atomic percentages (at %)			
	C	N	O	S
GO	69.3994	0.548963	29.0068	1.04484
rGO	87.8197	0	12.1352	0.045036
N/S_1:40	87.0422	0.272711	12.4908	0.194368
Pyrrole/N/S_1:1:40	87.2772	0.785251	11.7115	0.22608
Pyrrole/N/S_20:1:40	86.4843	4.39095	8.76828	0.356496
Pyrrole/N/S_40:1:40	83.5699	7.89829	8.21087	0.320896

A detail scan of each element was conducted to gain insight into the chemical nature of the NS-G. Data obtained from the high resolution spectra in the relevant regions are presented in Table 3 and Fig. 3.3-5. The C 1s binding energy spectrum was deconvoluted to five peaks (Fig. 3.3) with the main peak with binding energy of 284 eV which corresponds to sp^2, suggesting C=C is the main carbon bonding configuration, which creates the graphitic structure that is most of the C atoms still remained in the conjugated graphene system. Similar results were recorded by Y.wang et al, [53]. Second most intensed peak with B.E of 284.7 eV correspond to sp^3 carbon. The remaining three peaks with B.E of 286 eV, 287 eV and 288 eV correspond to hydroxyl and epoxy groups (C-O) carbonyl group (C=O) and carboxylic

(O-C=O) groups. However upon modification with NH_4SCN, to produce the nanocomposites, it is seen that the peaks at 286 eV and 287 eV drop indicating overlapping of C-O and C=O with C-N and C=N respectively. This also explains the deoxygenation of GO and the doping of GO with N. The peak at 290 eV is the satellite of sp^2 aromatic bonds due to π-π* shake-up.

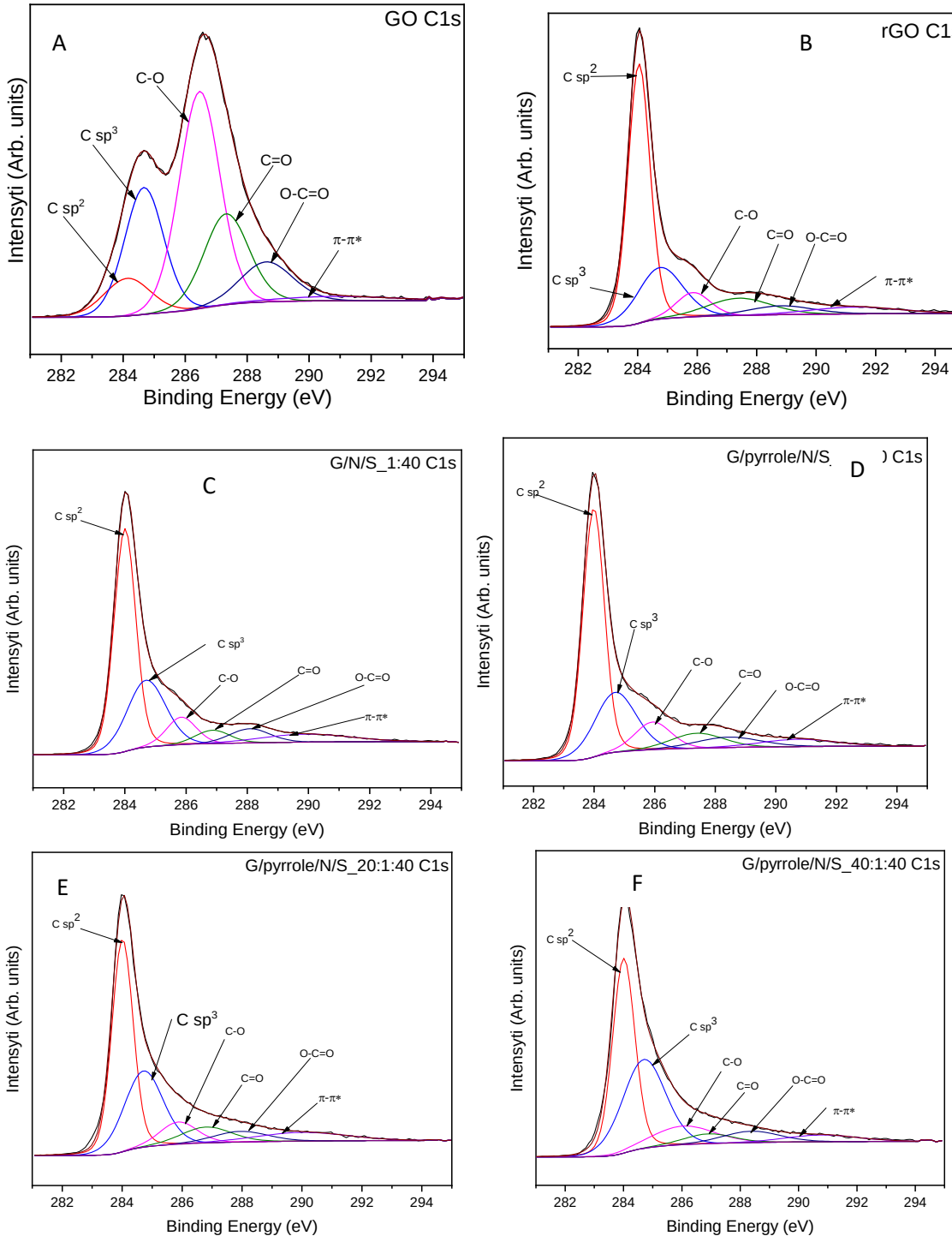

Fig 3.3 XPS of C 1s for (A) GO (B) rGO (C) NS-G 1:40 (D) NS-G 1:1:40. (E) NS-G 20:1:40. (F) NS-G 40:1:40

The deconvolution of N 1s shows several nitrogen functional groups in N/S-G-doped carbon. These include pyridinic-N, pyrrolic N (N5), quaternary N (NQ) and pyridine-N oxide with B.E at peaks 397 eV, 399 eV, 400 eV and 403 eV respectively. Fig. 3.4 shows the N functional groups for NS-G 20:1:40 and NS-G 40:1:40. The electrochemical performance of the NS-G is directly affected by the electrochemical properties of these four nitrogen functional groups. Therefore, the content of these four nitrogen functional groups in the N/S-G catalysts is a crucial characteristic, [54]. N6 refers to nitrogen atoms at the edge of graphene planes, which is bonded to two carbon atoms and donates one p-electron to the aromatic π-system; N5 refers to nitrogen atoms that are bonded to two carbon atoms and contribute to the π-system with two p-electrons.; quaternary nitrogen is also called ‘‘graphitic nitrogen’’ or ‘‘substituted nitrogen’’, in which nitrogen atoms are incorporated into the graphene layer and replace carbon atoms within a graphene plane, and is the dominant component at high temperature. The pyridinic and pyrrolic N are always located at the graphitic edge, whereas quaternary N can be both ‘‘edge-N’’ and ‘‘bulk-like-N’’; N-oxides of pyridinic-N (labeled as N4, pyridinic–(N+ –O) are bonded to two carbon atoms and one oxygen atom, [55-57]. These groups were absent in GO, so, the successful incorporation of nitrogen atoms in GO particles was confirmed by the presence of these groups in NS-G, [54]. In this study, it is seen that N5 has the most intense peak and it increases with increasing concentration of pyrrole. N6 was also seen to increase with increasing pyrrole concentration. It has been reported that pyridinic N and graphitic N can more strongly contribute to the catalytic activity. The higher percentages of pyridinic N and graphitic N in the NSG was assigneded to the structure of the N source polypyrrole that was easily converted to pyridinic N and graphitic N, which would bring better electrocatalytic performance, [22].

Table 3: XPS analysis results obtained from high resolution spectra of GO rGO and NS-G nanocomposites.

Sample	C1s						N1s				S2p	
	Csp^2	Csp^3	C-O/ C-N	C=O/ C=N	O-C=O	π-π*	N6	N5	NQ	Piridine oxide	$C\text{-}S_n$[c]/ S-S	$-SO_n$[a]
GO	284,2 (13,57)	284.7 (19,71)	286.5 (32,70)	287.3 (21,59)	288,6 (10,50)	291,0 (1,93)	n.d.	n.d.	n.d.	n.d.	n.d.	168,5 (100)
rGO	284,04 (52,20)	(284.8) 20,53	286.00 (7,32)	287.4 (9,67)	288.81 (4,94)	291.32 (5,34)	n.d.	n.d.	n.d.	n.d.	n.d.	168,63 (100)
NSG 1:40	284,0 (49,14)	284,7 (25,54)	285.84 (8,09)	286,86 (4,58)	288.20 (5,62)	290,10 (7,02)	n.d.	399,33 (31,83)	400,99 (68,17)	n.d.	164,75 (27,98)	168,93 (72,02)
Pyrrole NSG 1:1:40	284.01 (49,96)	284.7 (22,61)	285.93 (9,15)	287.4 (7,18)	288.43 (6,10)	290,73 (4,99)	n.d.	399,12 (37.15)	400,25 (62.85)	n.d.	164,69 (27.47)	168,88 (72.53)
Pyrrole NSG 20:1:40	284.01 (43,84)	284.72 (27,90)	285.88 (7,84)	286.81 (7,55)	287.94 (5,46)	290.10 (7,41)	397,42 (2.4)	399,39 (67.74)	400,52 (22.42)	403,44 (7.44)	164.57 (35.81)	168.61 (64.19)
Pyrrole NSG 40:1:40	284.01 (40,47)	284.7 (34,53)	286,04 (10,43)	286,91 (4,33)	288,37 (5,86)	290,78 (4,38)	397.5 (3,42)	399.47 (71.64)	400.61 (19.74)	403.52 (5.2)	164.69 (26.03)	168.87 (73.97)

[a]For 2p orbitals the B.E. of $2p_{3/2}$ orbital is presented; [b] Area of each component relative to the total core level peak area in percentage;[c] n = 1 or 2; n.d. – not detected; N6 – piridinic N; N5 – pyrrolic N; NQ-graphitic N.

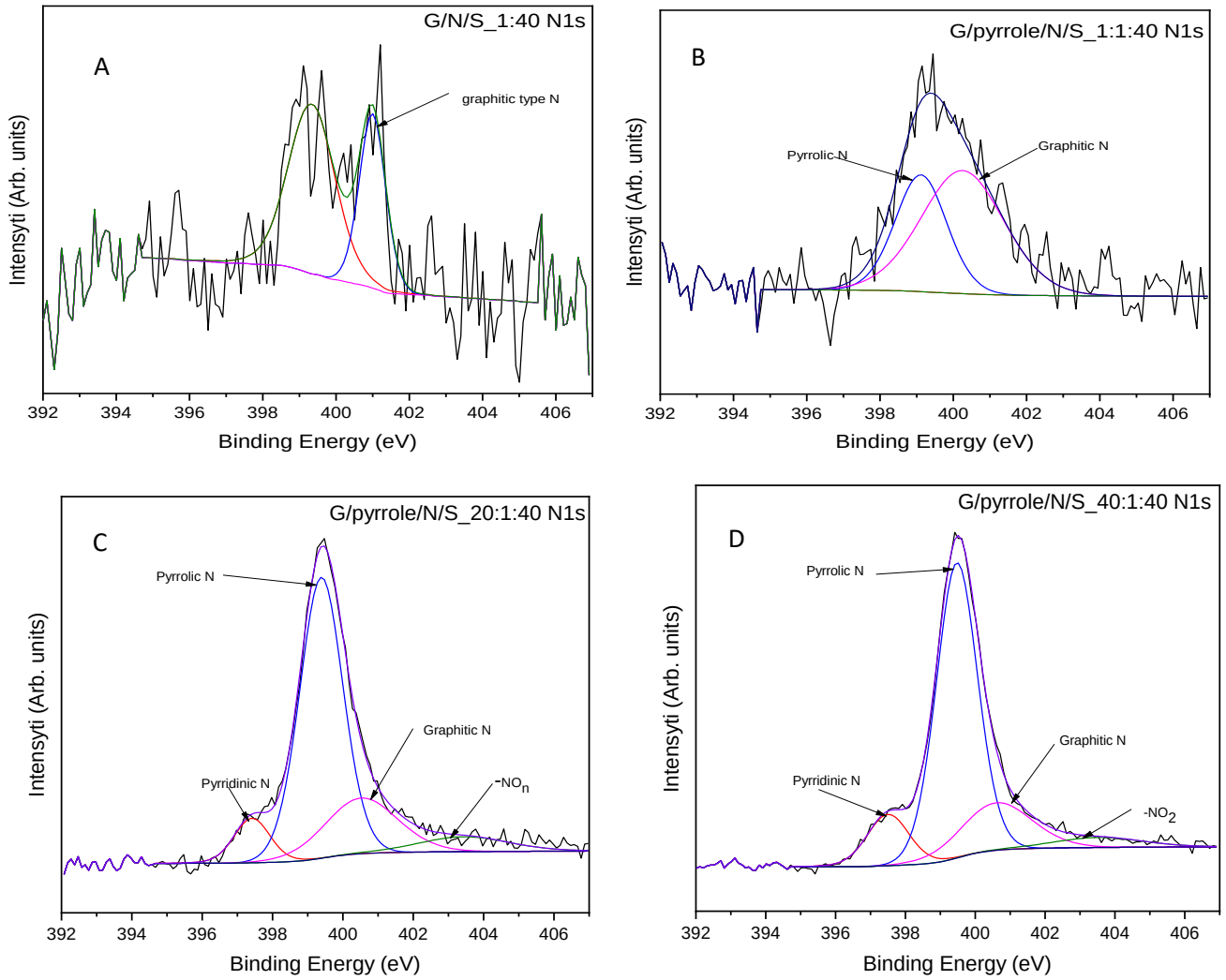

Fig 3.4 N 1s XPS showing N functional groups for (A) NS-G 1:40 and (B) NS-G 1:1:40. (C) NS-G 20:1:40. (D) NS-G 40:1:40.

The deconvolution of S 2p shows S bands in S 2p region, appear in the form of doublets, due to the degeneration in the B.E. of $2p_{3/2}$ and $2p_{1/2}$ orbitals. From the high resolution of the nanocomposites, two peaks can be assign to C-S-C or S-S (164.8 eV) with lower energy and higher energy oxidized sulfur moiety, $-SO_n$ (168 eV) species are seen. These peaks are seen in doublets of S $2p_{1/2}$ and $s2p_{3/2}$ as seen on the Fig. 3.5. C-S-C species is known to bring more catalytically active sites for electrocatalytic performance while $-SO_n$ occur at the edges of graphene. $-SO_n$ was seen to have more intensed peak than $C-S_n-C$ implying it was the dominant state of sulphur. The peak intensity of $-SO_n$ remained constant from GO to all nanocomposites this suggest that the presence of this functional group is due to residual sulfuric acid during preparation of GO. Whereas C-S-C was absent in GO but present in the nanocomposite suggesting that its presence is as a result of functional modification. Moreover, the co-doping of N and S altered the local chemical environment, generating more active sites towards electrocatalysis for sensing. Consequently, the electrochemical performance was expected to be enhanced, [22]

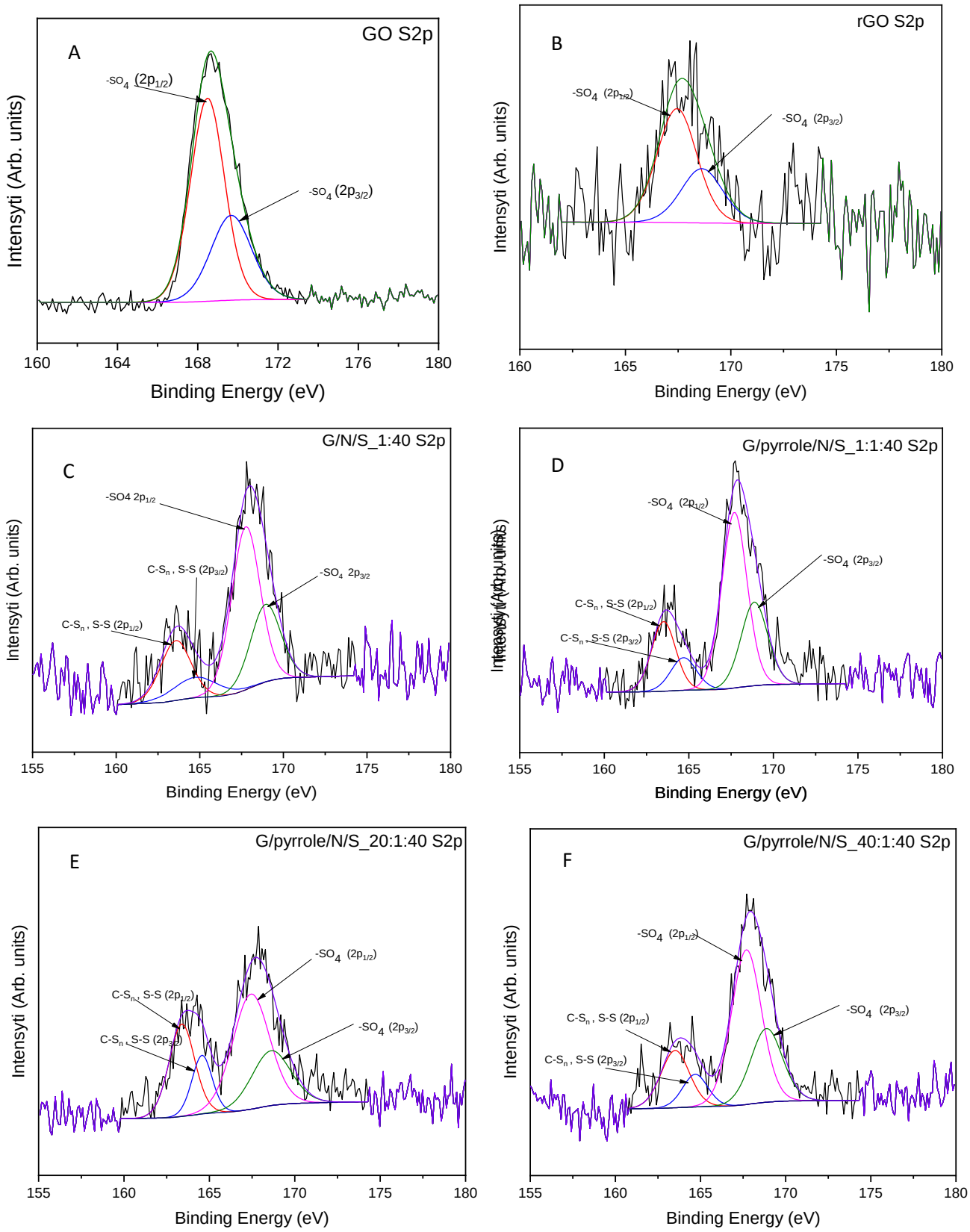

Fig. 3.5 S 2p XPS showing S functional groups (A) GO, (B) rGO (C) NS-G1:40 (D) NS-G 1:1:40 (E) NS-G 20:1:40 and (F) NS-G 40:1:40.

3.1.4. Raman analysis

The Raman analysis was conducted to further investigate the structure of the nanocomposites. All samples including GO and rGO demonstrated two peaks corresponding to the D and G bands, (Fig. 3.6). The G band which refers to the degree of graphitization is a doubly degenerate of in-plane transverse optic and longitudinal optic (iTO and LO) phonon mode (E_{2g} symmetry) at the t Brillouin zone (BZ) center that is Raman active for sp^2 carbon networks. The presence of a G band in the Raman spectra, indicates the presence of sp^2 carbon networks in the sample, this band arises from the bond stretching of all sp^2-bonded pairs. The G-band is the only band coming from a normal first order Raman scattering process in graphene, [58-60].

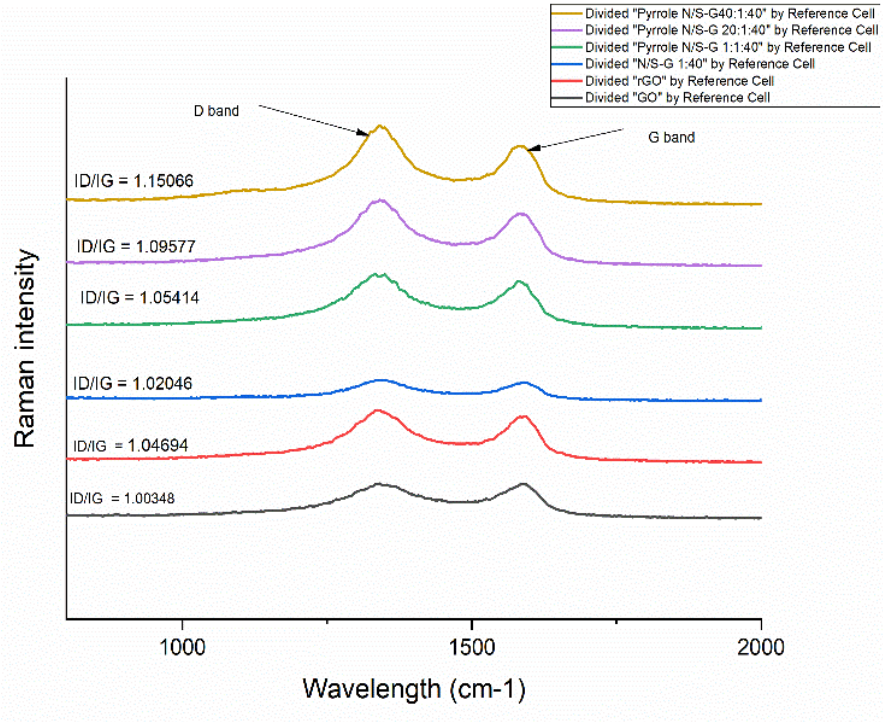

Fig. 3.6 .Raman spectra showing GO, rGO and NS-G nanocomposites showing the D and G and their various I_{D1}/I_G ratio.

The D band correlates with the amount of structural defects or disorder in the sp^2 hybridized carbon material, it originates from a second-order process, involving one iTO phonon and one defect, [56 - 58].This mode is forbidden in perfect graphite and it only becomes active in the presence of a disorder. The D mode is dispersive; it varies with photon excitation energy, even when the G peak is not dispersive. Its intensity is strictly connected to the presence of six fold aromatic rings. It is seen from the table below that the more modified our material is the greater the D band indicating more disorder in the sp^2 network. The I_D/I_G ratio represents structural disorder in graphitic materials. The I_{D1}/I_G ratio increases with increased modification, that is, it increases with increased concentration of pyrrole as seen in Fig. 3.6. The I_D/I_G of the nanocomposites were higher than that of GO. These results indicate a significant level of disorder and the presence of defects in the prepared catalyst materials. Similar result was reported by Dang et al, [60] and Zhang et al, [62].

3.2. Electrochemical analysis

Cyclic voltammetry (CV) was conducted to measure the electrochemical activity of the various samples in the presence and absence of glucose. The working potential was observed at 0.6 V. The CV curves of GO and NS-G 40:1:40 in PBS + 0.1 M KCl at a scan rate of 5 mV/s are shown in Fig. 3.7. Both GO and NS-G 40:1:40 electrodes show a redox peak at the same potential window. However, the peak currents of NS-G 40:1:40 electrode were higher (31.18 µA and 27.725 µA) with and with no glucose respectively than those of GO (25.068 µA and 18.127 µA). The cathodic peak current and anodic peak current are assigned to the reduction of GOD (FAD) and the oxidation of GOD ($FADH_2$), respectively. This suggests that the facile DET process occurs from the redox site of the enzyme ($FAD/FADH_2$ redox center) to GOD/NS-G graphite electrode. The enhanced redox peak currents of NS-G 40:1:40 is probably due to the introduction of heteroatoms into the graphene sheets, thereby introducing more electrocatalytic active sites to facilitate transfer of charges, resulting to high electrocatalytic performance of the modified GOD/NS-G graphite electrode hence, faster DET process of GOD at the graphite electrode.

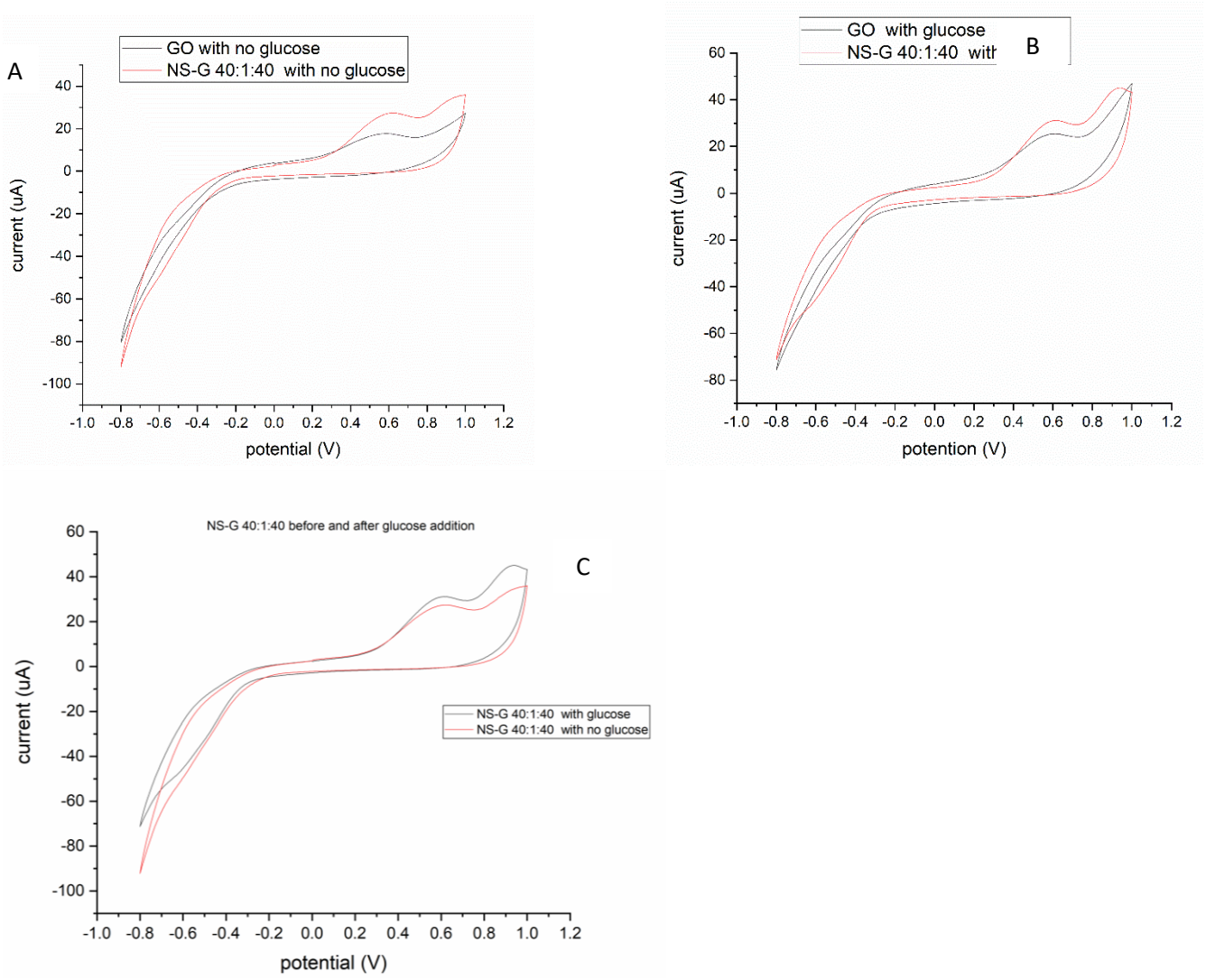

Fig. 3.7. CV for GO and NS-G 40:1:40. A) In the absence of glucose. B) In the presence of glucose. (C) NS-G in the presence and absence of glucose. Plot obtained by Origin pro 2018

Fig. 3.7.C shows cyclic voltammetry for NS-G before and after addition of 0.1 M glucose at a scan arte of 5 mVs^{-1}. In order to work as a catalyst, GOD requires a redox cofactor—flavin adenine dinucleotide (FAD). FAD works as the initial electron acceptor and is reduced to $FADH_2$ as shown in equation 1.

$$GOD\ (FAD) + 2e^- + 2H \rightarrow GOD\ (FADH)_2 \qquad (1)$$

In the absence of glucose, GOD ($FADH_2$) catalyzes the reduction of dissolved oxygen in buffer solution to hydrogen peroxide (H_2O_2) followed by the regeneration of GOD (FAD). H_2O_2 is then oxidized at the anode producing oxygen according to the following equation (2 and 3), [63- 64]

$$GOD\ (FADH_2) + O_2 \rightarrow GOD\ (FAD)^+ + H_2O_2 \qquad (2)$$

$$H_2O_2 \rightarrow 2H^+ + O_2 + 2e \qquad (3)$$

Upon the addition of glucose, an increased in anodic and cathodic peak currents was observed signifying glucose oxidation as shown in equation (4), suggesting that glucose restrains the above reaction due to the newly appeared reaction between GOD (FAD) and glucose. The anode easily recognizes the number of electron transfers, and this electron flow is proportional to the number of glucose molecules.

$$Glucose + GOD\ ((FAD)^+ \rightarrow Glucolactone + GOD\ (FADH_2) \qquad (4)$$

Furthermore, chronoamperometry response for the NS-G 40:1:40 electrode upon successive addition of 0.1 M glucose in PBS + KCl (0.1 M, pH 7.0) at a constant potential of 0.6 V versus Ag/AgCl was carried out as shown in Fig. 3.8. Addition of aliquots of 0.1 M glucose shows an increased in current until it plateaus at a given concentration of 0.1 M glucose due to saturation of the electrode.

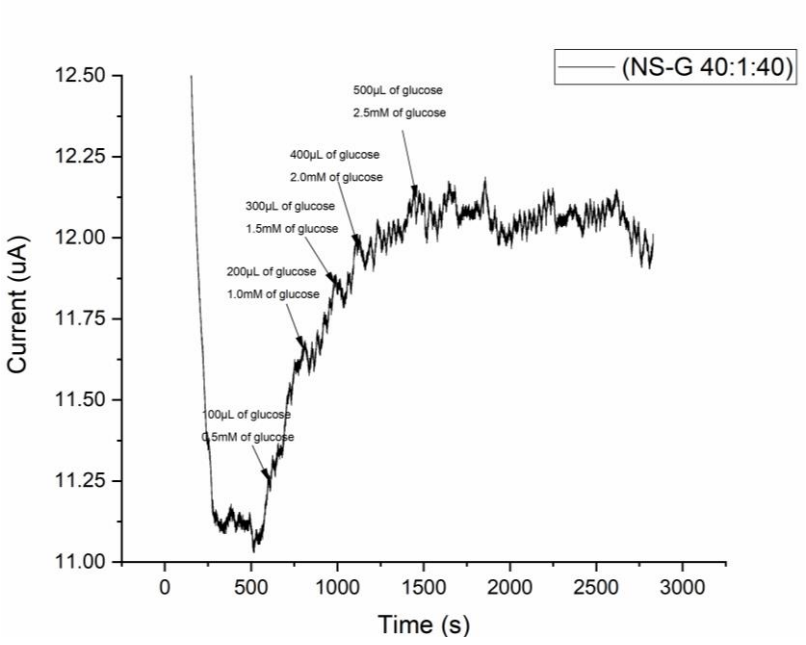

Fig 3.8. Amperometric response of GOD/NS-G graphite electrode to successive addition of different glucose concentrations.

Fig 3.8. Amperometric response of GOD/NS-G graphite electrode to successive addition of different glucose concentrations to oxygen-saturated PBS (0.1 M, pH=7.0) at an applied potential of 0.6 V. A calibration curve of current versus the concentration of glucose with a linear response of 0.5 mM to 2.5 mM and a correlation coefficient of 0.9621 as shown on Table 4; Fig. 3.9., was displayed by this biosensor (NS-G 40:1:40). From the slope, the sensitivity and limit of detection of the biosensor were obtained from equations 5 and 6 respectively.

Sensitivity = slope of the calibration curve/ Area of the graphite rod (5)

Where area of graphite rod = 0.070686 cm^2 and slope = 0.4911 $\mu A*mM^{-1}$

Limit of detection (LOD) = 3 X standard deviation / slope (6)

Standard deviation = 0.06842

Table 4 shows concentration of glucose versus current obtained from chronoamperometry plot.

Concentration of glucose (mM)	NS-G 40:1:40 Current (µA)
0.5	0.20
1.0	0.62
1.5	0.82
2.0	0.95
2.5	1.08

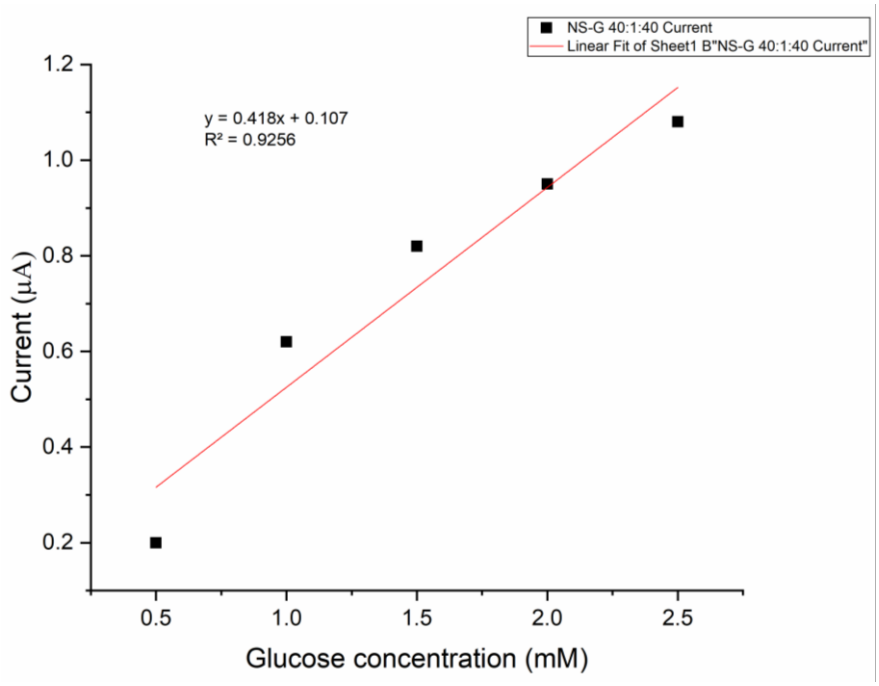

Fig. 3.9. Calibration plot of current versus glucose concentration of NS-G 40:1:40. Plot obtained by Origin pro 2018

The sensitivity was calculated to be 6.9476 µA*mM-1*cm^{-2}, which is higher than values reported for GOD/PtNPs/CNTs/nafion/GCE (2.11 µA mM^{-1}) and GOD/PtNPs/CNTs/carbon paste (0.28 µA $mM^{=1}$), [66]. This shows better results than some electrode nanomaterial reported on Table 5, for the construction of GOD-based glucose biosensors. The detection limit was determined to be 0.4911 mM signal to noise ratio of 3. This sensor could be applicable for blood glucose detection. Glucometers from brands like One Touch Verio and OnCall Plus are known to have higher detection range for blood glucose of 1.11 mM to 33.3 mM below which they can detect but not quantify the amount of glucose present.

Table.5. Comparison of the sensing performances of state-of-the-art nanomaterials for the construction of GOD-based glucose biosensors

Electrode material	Linear range	Sensitivity µA$mM^{-1}cm^{-2}$	Detection limit µM (S/N=3)	Ref
Nitrogen/sulphur-Graphene	0.01 to 17.2 mM	145.7	0.6	41
Graphene/multiwalled–carbon nanotube AuNP	10 µM–2 mM	0.695	4.1	68
$SiPy^{+}Cl^{-}$/CuTsPc	1-10 mM	13.97	0.16	69
AuNPs-hydrogel	0.1-10 mM	100	0.37	70
Au-PtNPs/CNTs/CS	0.001-7.0 mM	8.53	0.2	71
CDH/GA/4-APh,4-MBA/AuNPs/GC	0.02 to 30 mM	3.1	6.2	72
NS-G	0.5 – 2.5 mM	6.9476	0.4911	My work

$SiPy^{+}Cl^{-}$/CuTsPc: 3-*n*-propylpyridinium silsesquioxane polymer ($SiPy^{+}Cl^{-}$) and copper (II) tetrasulfophthalocyanine (CuTsPc). Au-PtNPs/CNTs/CS = Gold-platinum alloy nanoparticles (Au-PtNPs)/ multiwall carbon nanotubes/ chitosan film.

It has been shown that N and S co-doping improves electrical conductivity, which facilitates the DET process between the redox centers of the GOD and the surface of graphite rod. The defective sites of N, S co-doped graphene could provide more electrocatalytic active sites for oxygen absorption and glucose oxidation, [67]. Consequently, the electrocatalytic activity of doping N and S leads to the better glucose sensing performances of GOD/NS-G graphite rod. However, further investigations on the better deposition of material on electrode surface, detailed relationship between electrocatalytic activities of GOD/glucose reaction, and NS-G doping species, especially graphitic-N and -C-S_n-C- 2p, need to be carried out to better understand the reason behind these observations.

CONCLUSIONS

The absence of band-gap in graphene restricts its application in the field of sensing, and electrocatalysis. This problem can be undone through the functionalization process by doping graphene with heteroatoms. The dual doping of graphene with heteroatoms viz N and S produces a graphene nanocomposite (NS-G) that is capable decorating the graphene planar sheet and introduce a change in the Fermi level, engendering the doping effects and opening the band gap of the graphene thereby enahancing the electrochemical activity in electrochemical systems.

- Using Hummers method GO was synthesized and NS-G nanocomposite was prepared by hydrothermal treatment"
- SEM analysis revealed the material had undergone some morphological changes subsequent to modification. The nanocomposite was seen to have rough curled edges due to defective sites form during heteroatoms doping.
- The FTIR spectra confirm the presence of C=N, CN, and C-S bonds indicating successful co-doping of nitrogen and sulphur atoms into the structure of GO. XPS analysis further confirm a successful doping by displaying peaks of C, O, N, and S. The atomic percentages for elemental analysis revealed decreased in oxygenated groups and increased in N and S groups, thus, these oxygenated groups were replaced by N and S during doping process.
- Raman spectra, revealed structural defects in the sp^2 hybridized graphene structure. The I_D/I_G ratio increases with increased modification indicating disorder in the nanocomposite.
- The nanocompposite was observed to have higher oxidation and reduction peaks than the control GO both before and after glucose addition. Higher oxidation current was recorded upon glucose addition than before. This material had a linear range of 0.5 mM to 2.5 mM, a sensitivity 6.9476 $\mu A*mM^{-1}*cm^{-2}$, and limit of detection of 0.4911 µM. These results show this nanocomposite is a potential material for glucose biosensors.

REFERENCES

1. A. Madni, S. Noreen, I. Maqbool, F. Rehman, A. Batool, P. M. Kashif, M. Rehman, N. Tahir and M. I. Khan, Graphene-based nanocomposite, synthesis and their theranostic applications, Journal of Drug Targeting. 10 (2018) 858– 883. DOI: 10.1080/1061186X.2018.1437920
2. S. Kaushal, M. Kaur, N. Kaur, V. Kumari, & P. P. Singh, Heteroatom-doped graphene as sensing materials: a mini review. RSC Advances. 10; 48 (2020) 28608–28629. doi:10.1039/d0ra04432f
3. J. Wang, X. W. Sun, A. Wei, Y. Lei, X. Cai, C.M. Li, Z. L. Dong, Zinc oxide nanocomb biosensor for glucose detection. Journal of Applied Physics Letters. 88 (2006) 233106. DOI:10.1063/1.2210078
4. X. Wang, G. Sun, P. Routh, D.-H. Kim, W. Huang, P. Chen, Heteroatom-doped graphene materials: syntheses, properties and applications. Journal of Chemical Society Review. 43 (2014) 7067. https://doi.org/10.1039/C4CS00141A
5. N. J. Coville, S. D. Mhlanga, E. N. Nxumalo, A. Shaikjee, A review of shaped carbon nanomaterials. South African Journal of Science. 107 (2011) 01-15. DOI: 10.4102/sajs.v107i3/4.418
6. Q. L. Yan, M. Gozin, F. Q. Zhao, A. Cohen, S. P. Pang, Highly Energetic Compositions Based on Functionalized Carbon Nanomaterials. Nanoscale. 8; 9 (2016) 4799-4851. https://doi.org/10.1039/C5NR07855E
7. A. Al-Jumaili, S. Alancherry , K. Bazaka and V. J. Mohan, Review on the Antimicrobial Properties of Carbon Nanostructures. Multidisciplinary Digital Publishing Institute MDPI journal. Materials. 10 (2017) 1066. https://doi.org/10.3390/ma10091066
8. Y. Wu, T. Yu, Two-dimensional Carbon: Fundamental Properties, Synthesis, Characterization, and Applications, Pan Stanford Publ., Singapore (2014).
9. V. Georgakilas, J. A. Perman, J. Tucek, R. Zboril, Broad Family of Carbon Nanoallotropes: Classification, Chemistry, and Applications of Fullerenes, Carbon Dots, Nanotubes, Graphene, Nanodiamonds, and Combined, Super structures Chemical Reviews. 115 (2015) 4744-4822. DOI: 10.1021/cr500304f
10. I. Suarez-Martinez, N. Grobert, C. P. Ewels, Nomenclature of sp2 carbon nanoforms, Carbon. 50; 3 (2012) 741-747. 10.1016/j.carbon.2011.11.002
11. C. Sainz-Urruela , S. Vera-López, M. P. S. Andrés, and A. M. Díez-Pascual, Graphene-Based Sensors for the Detection of Bioactive Compounds: A Review, International journal of molecular science. 22 (2021) 3316. . https://doi.org/ 10.3390/ijms22073316
12. T. Kuila, S. Bose, A. K. Mishra, P. Khanra, N. H. Kim, J. H. Lee, Chemical functionalization of graphene and its applications, Progress in Materials Science. 57; 7 (2012) 1061-1105. DOI10.1016/j.pmatsci.2012.03.002
13. U. K. Sur, International Journal of Electrochemistry 2012 (2012) 12.
14. J. Zhu, J. Wang, J. Hou, Y. Zhang, J. Liub and B. Van der Bruggen, Graphene-based antibacterial polymeric membrane: A Review, Journal of material chemistry A, 5 (2017) 6776. https://doi.org/10.1039/C7TA00009J

15. M. Islama, S. S. Ahmedb, M. Rashidc , M. Akandad, Mechanical and Thermal Properties of Graphene over Composite Materials: A Technical Review, Journal of Casting & Materials Engineering, 3; 1 (2019) 19–30. http://dx.doi.org/10.7494/jcme.2019.3.1.19
16. K. P. Loh, Q. Bao, P. K. Ang, J. Yang, The chemistry of graphene, Journal of Material Chemistry. 20, (2010) 2277–89. https://doi.org/10.1039/B920539J
17. W. Bao, F. Miao, Z. Chen, H. Zhang, W. Jang, C. Dames and C. N. Lau, Controlled ripple texturing of suspended graphene and ultrathin graphite membranes. Nature Nanotechnology. 4; 9 (2009) 562. DOI: 10.1038/nnano.2009.191
18. R. Sharma, N. Nair and M. S. Strano, Structure-Reactivity Relationships for Graphene Nanoribbons. Journal of Physical Chemistry C. 113; 33 (2009) 14771. https://doi.org/10.1021/jp904814h
19. R. D. Dreyer, S. Park, C. W. Bielawski, R.S. Ruoff, The chemistry of graphene oxide, Journal of Chemical Review Society. 39 (2010) 228–40. https://doi.org/10.1039/B917103G
20. H. Fan, L. Wang, K. Zhao, N. Li, Z. Shi, Z. Ge, et al., Fabrication, mechanical properties, and biocompatibility of graphene reinforced chitosan composites, Biomacromolecules. 11 (2010) 2345–51. https://doi.org/10.1021/bm100470q
21. J. Gaidukevic, J. Razumiene, I. Sakinyte, S. L. H. Rebelo, J. Barkauskas, Study on the structure and electrocatalytic activity of graphene-based nanocomposite materials containing (SCN)n. Carbon. 118 (2017) 156-167. https://doi.org/10.1016/j.carbon.2017.03.049
22. Z. Huang, H. Zhou, W. Yang, C. Fu, L. Chen, and Y. Kuang, Three-Dimensional Hierarchical Porous Nitrogen and Sulfur-Codoped Graphene Nanosheets for Oxygen Reduction in both Alkaline and Acidic Media, ChemCatChem. 9 (2017) 987 – 996. https://doi.org/10.1002/cctc.201601387
23. J. Wu, W. Pisula and K. Mullen, Graphenes as potential ¨ material for electronics, Chemical Review, 107 (2007) 718–747. https://doi.org/10.1021/cr068010r
24. N. G. Sahoo, Y. Pan, L. Li and S. H. Chan, Graphene-based materials for energy conversion, Advanced Material. 24 (2012) 4203–4210. https://doi.org/10.1002/adma.201104971
25. K. A. Ritter and J. W. Lyding, The influence of edge structure on the electronic properties of graphene quantum dots and nanoribbons, Nature. Material. 8 (2009) 235–242. https://doi.org/10.1038/nmat2378
26. V. Georgakilas, M. Otyepka, A.B. Bourlinos, V. Chandra, N. Kim, K.C. Kemp, P. Hobza, R. Zboril, K.S. Kim, Functionalization of graphene: covalent and non-covalent approaches, derivatives and applications, Chemical Review. 112 (2012) 6156-6214. https://doi.org/10.1021/cr3000412
27. X. Huang, Z. Yin, S. Wu, X. Qi, Q. He, Q. Zhang, H. Zhang, Graphene-Based Materials: Synthesis, Characterization, Properties, and Applications, Small. 7; 14 (2011) 1876–1902. doi:10.1002/smll.201002009
28. M. J. Park, J. K. Lee, B. S. Lee, Y.W. Lee, I.S. Choi, & S. Lee, Covalent Modification of Multiwalled Carbon Nanotubes with Imidazolium-Based Ionic Liquids: Effect of Anions on Solubility, Chemistry of Materials. 18; 6 (2006) 1546–1551. doi:10.1021/cm0511421

29. C. Han, & Y.-J. Xu, The surface chemistry of graphene-based materials: functionalization, properties, and applications, Surface Science of Photocatalysis. 2020, 453–474. doi:10.1016/b978-0-08-102890-2.00014-2
30. E. Bekyarova, M.E. Itkis, P. Ramesh, C. Berger, M. Sprinkle, Herr WA, et al., Chemical modification of epitaxial graphene: spontaneous grafting of aryl groups, Journal of American Chemical Society. 131 (2009) 1336–7. https://doi.org/10.1021/ja8057327
31. N. Nakayama-Ratchford, S. Bangsaruntip, X. Sun, K. Welsher, H. Dai, Noncovalent functionalization of carbon nanotubes by fluorescein–polyethylene glycol: supramolecular conjugates with pH-dependent absorbance and fluorescence, Journal of American Chemical Society. 129 ((2007) 2448–9. https://doi.org/10.1021/ja068684j
32. Y.-L. Zhao, & J. F. Stoddart, Noncovalent Functionalization of Single-Walled Carbon Nanotubes, Accounts of Chemical Research. 42; 8 (2009) 1161–1171. doi:10.1021/ar900056z
33. D. C. Elias, R.R. Nair, T. M. G. Mohiuddin, S. V. Morozov, P. Blake, M.P. Halsall, K.S.Novoselov et al., Control of Graphene's Properties by Reversible Hydrogenation: Evidence for Graphane, Science. 323; 5914 (2009) 610–613. doi:10.1126/science.1167130
34. H. Yang, M. Chen, H. Zhou, C. Qiu, L. Hu, F. Yu, L. Sun, et al., Preferential and Reversible Fluorination of Monolayer Graphene. The Journal of Physical Chemistry C. 115; 34 (2011) 16844–16848. doi:10.1021/jp204573z
35. J.-F. Dai, G.-J. Wang, L. Ma and Ch.-K. Wu, Surface properties of graphene: relationship to graphene-polymer composites, Review Advanced Material Science. 40 (2015) 60-71
36. M. Peressi, Surface Functionalization of Graphene. In: Graphene Chemistry, (John Wiley & Sons, Ltd, 2013) p. 233.
37. S. Chen, M. B. Muller, K. J. Gilmore, G. G. Wallace and D. Li, Advanced Material. 20 (2008) 3557
38. Y. Wang, Y. Shao, D.W. Matson, J. Li, Y. Lin, Nitrogen-Doped Graphene and Its Application in Electrochemical Biosensing, ACS Nano, 4 (2010) 1790. https://doi.org/10.1021/nn100315s
39. H. Liu, Y. Liu, D. Zhu, Chemical doping of graphene, Journal of Material Chemistry. 21 (2011) 3335–3345 | 3335. https://doi.org/10.1039/C0JM02922J
40. Qi Y, Cao Y, Meng X, Cao J, Li X, Hao Q, Lei W, Li Q, Li J, Si W, Facile synthesis of 3D sulfur/nitrogen co-doped graphene derived from graphene oxide hydrogel and the simultaneous determination of hydroquinone and catechol, Sensors and Actuators. B. Chemical, 2018. https://doi.org/10.1016/j.snb.2018.09.067
41. G. Chen, Y. Liu, Y. Liu, Y. Tian, X. Zhang, Nitrogen and sulfur dual-doped graphene for glucose biosensor application, Journal of Electroanalytical Chemistry, 2014. doi: http://dx.doi.org/10.1016/ j.jelechem.2014.11.02
42. M. Desmulliez, Biosensors for the detection of waterborne pathogens. Waterborne Pathogens. Academic Press, 2014 189-229. https://doi.org/10.1016/B978-0-444-59543-0.00007-4.
43. K. R. Srivastava, S. Awasthi, P. K. Mishra, P. K. Srivastava, Biosensors/molecular tools for detection of waterborne pathogens. 2020. https://doi.org/10.1016/B978-0-12-818783-8.00013-X
44. Y. Zheng, Y. Jiao, L. Ge, M. Jaroniec, & S. Z. Qiao, Two-Step Boron and Nitrogen Doping in Graphene for Enhanced Synergistic Catalysis. Angewandte Chemie International. 52; 11 (2013) 3110–3116. doi:10.1002/anie.201209548

45. Y. Su, Y. Zhang, X. Zhuang, S. Li, D. Wu, F. Zhang, X. Feng, Low-temperature synthesis of nitrogen/sulfur co-doped three-dimensional graphene frameworks as efficient metal-free electrocatalyst for oxygen reduction reaction. CARBON, 2013, 62, 296 – 301. https://doi.org/10.1016/j.carbon.2013.05.067
46. H. Deng, M. Zhu, T. Jin, C. Cheng, J. Zheng, Y. Qian, One-step synthesis of nitrogen, sulphur-codoped graphene as electrode material for supercapacitor with excellent cycling stability, International Journal of Electrochemcal Science. 2020, 15; 16 – 25, doi: 10.20964/2020.01.13
47. M. S. Khan, R. Yadav, R. Vyas, A. Sharma, M. K. Banerjee, & K. Sachdev, Synthesis and evaluation of reduced graphene oxide for supercapacitor application. Materials Today: Proceedings, 2020 doi:10.1016/j.matpr.2020.05.403
48. S. Stankovich, R. D. Piner, S. T. Nguyen, & R. S. Ruoff, Synthesis and exfoliation of isocyanate-treated graphene oxide nanoplatelets, Carbon, 44; 15 (2006) 3342–3347. doi:10.1016/j.carbon.2006.06.004
49. T. Yang, F. Cai, X. Zhang and Y. Huang, Nitrogen and sulfur codoped graphene quantum dots as a new fluorescent probe for Au3+ ions in aqueous media, RSC Advances, 2015, 5; 130 (2015) 107340–107347. doi:10.1039/c5ra20060a
50. J. Song, X. Wang, & C-T. Chang C, Preparation and Characterization of Graphene Oxide. Journal of Nanomaterials, 2014 (2014) 1–6. doi:10.1155/2014/276143
51. M. E.Lipińska, J. P. Novais, S. L. H. Rebelo, B. Bachiller-Baeza, I. Rodríguez-Ramos, A. Guerrero-Ruiz, & C. Freire, Microwave-assisted silylation of graphite oxide and iron(III) porphyrin intercalation, Polyhedron. 81 (2014) *475–484.* doi:10.1016/j.poly.2014.07.003
52. R. A. Rochman, S. Wahyuningsih, A. H. Ramelan, & Q. A. Hanif, Preparation of nitrogen and sulphur Co-doped reduced graphene oxide (rGO-NS) using N and S heteroatom of thiourea. IOP Conference Series: Materials Science and Engineering. 509 (2019) 012119. doi:10.1088/1757899x/509/1/012119
53. Y. Wang, Y. Shao, D. W. Matson, J. Li, and Y. Lin, Nitrogen-Doped Graphene and Its Application in Electrochemical Biosensing. ACS NANO, 4; 4 (2010) https://doi.org/10.1021/nn100315s
54. S. Zhuang, E. S. Lee, L. Lei, B. B. Nunna, L. Kuang and Wen Zhang, Synthesis of nitrogen-doped graphene catalyst by high energy wet ball milling for electrochemical systems, International Journal of Energy Research, 2016, © 2016 John Wiley & Sons, Ltd. https://doi.org/10.1002/er.3595
55. Y. Shao, S. Zhang, M. H. Engelhard, G. Li, G. Shao, Y. Wang, J. Liu, I. A. Aksayc and Y. Lin, Nitrogen-doped graphene and its electrochemical applications, Journal of Material science Chem, 20 (2010) 7491–7496 | 7493. https://doi.org/10.1039/C0JM00782J
56. L. Lai, J. R. Potts, D. Zhan, L. Wang, C. K. Poh, C. Tang, H. Gong, Z. Shen, J. Linc and R. S. Ruoff, Exploration of the active center structure of nitrogen-doped graphene-based catalysts for oxygen reduction reaction, Journal of Energy Environmental Science, 5 (2012) 7936 https://doi.org/10.1039/C2EE21802J
57. Y. H. Lee, K. Chang, C. Hu, Differentiate the pseudocapacitance and double-layer capacitance contributions for nitrogen-doped reduced graphene oxide in acidic and alkaline electrolytes, Journal of Power Sources, 227 (2013) 300-308. https://doi.org/10.1016/j.jpowsour.2012.11.026

58. M. A. Pimenta, G. Dresselhaus, M. S. Dresselhaus, L. G. Cançado, A. Jorio, & R. Saito, Studying disorder in graphite-based systems by Raman spectroscopy, Phys. Chem. Chem. Phys., 9; 11 (2007) 1276–1290. doi:10.1039/b613962k
59. L. M. Malard, M. A. Pimenta, G. Dresselhaus, & M. S. Dresselhaus, Raman spectroscopy in graphene, Physics Reports. 473; 5-6 (2009) 51–87. doi:10.1016/j.physrep.2009.02.003
60. F. Dang, W. Zhao, P. Yang, H. Wu, & Y. Liu, Nitrogen and sulfur co-doped hierarchical graphene hydrogel for high-performance electrode materials, Journal of Applied Electrochemistry, 2020, doi:10.1007/s10800-020-01404-5
61. R. Sibul, E. Kibena-Põldsepp, U. Mäeorg, M. Merisalu, A. Kikas, V. Kisand, K. Tammeveski, Sulphur and nitrogen co-doped graphene-based e lectrocatalysts for oxygen reduction reaction in alkaline medium, Electrochemistry Communications, (2019) 106603. doi:10.1016/j.elecom.2019.106603
62. J. Zhang, J. Wang, Z. Wu, S. Wang, Y. Wu, and X. Liu, Heteroatom (Nitrogen/Sulfur)-Doped Graphene as an Efficient Electrocatalyst for Oxygen Reduction and Evolution Reactions, Multidisciplinary Digital Publishing Institute, Catalysts, 8, (2018) 475. doi:10.3390/catal8100475
63. F.-H. Yoo and s.-Y. Lee, Glucose biosensors: An overview of use in clinical practice. Sensors. 10 (2010) 4558-4576; doi:10.3390/s100504558
64. J. Wang, Electrochemical Glucose Biosensors, Chem. Review. 108, (2008) 814−825. DOI: 10.1021/cr068123a
65. C. Chen, Q. Xie, D. Yang, H. Xiao, Y. Fu, Y. Tan and S. Yao, Recent advances in electrochemical glucose biosensors, Royal society of Chemistry Advanced, 3 (2013) 4473–4491 | 4473 DOI: 10.1039/c2ra22351a
66. S. Hrapovic, Y. Liu, K.B. Male, J.H.T. Luong, Electrochemical biosensing platforms using platinum nanoparticles and carbon nanotubes, Anal. Chem. 76 (2004) 1083–1088. https://doi.org/10.1021/ac035143t
67. L. Lai, J.R. Potts, D. Zhan, L. Wang, C.K. Poh, C. Tang, H. Gong, Z. Shen, J. Lin, R.S. Ruoff, Energ. Exploration of the active center structure of nitrogen-doped graphene-based catalysts for oxygen reduction reaction, Energy and Environtal Science, 5; 7 (2012) 7936. https://doi.org/10.1039/C2EE21802J
68. R. Devasenathipathy, V. Mani, S.-M. Chen, S.-T. Huang, T.-T. Huang, C.-M. Lin, B.-J. Chen et al., Glucose biosensor based on glucose oxidase immobilized at gold nanoparticles decorated graphene-carbon nanotubes, Enzyme and Microbial Technology. 78 (2015) 40–45. doi:10.1016/j.enzmictec.2015.06.006
69. C. G. De Jesus, D. Lima, V. dos Santos, K. Wohnrath, & C.A. Pessôa, Glucose biosensor based on the highly efficient immobilization of glucose oxidase on layer-by-layer films of silsesquioxane polyelectrolyte. Sensors and Actuators B. Chemical. 186 (2013) 44–51. doi:10.1016/j.snb.2013.05.063
70. V.A. Pedrosa, J. Yan, A.L. Simonian, A. Revzin, Micropatterned Nanocomposite Hydrogels for Biosensing Applications. Electroanalysis, 23, (2011) 1142. Doi: 10.1002/elan.201000654
71. X. Kang, Z. Mai, X. Zou, P. Cai, & J. Mo, A novel glucose biosensor based on immobilization of glucose oxidase in chitosan on a glassy carbon electrode modified with gold–platinum alloy

nanoparticles/multiwall carbon nanotubes, Analytical Biochemistry, 369; 1 (2007) 71–79. doi:10.1016/j.ab.2007.07.005
72. R. S. Singh, T. Singh, & A. K. Singh, Enzymes as Diagnostic Tools. Advances in Enzyme Technology, 2019, 225–271. doi:10.1016/b978-0-444-64114-4.00009-1

SUMMARY

Graphene a two-dimensional one atom thickness of graphite comprises of sp^2 carbon atoms which are tightly packed into a honeycomb crystal lattice. This compound has remarkable physical, chemical, and mechanical properties with values that surpass those obtained in any other materials, enabling them to be used in a wide range of applications. Despite these exceptional properties this compound possess, having a zero band-gap restrain its use in electrocatalaysis and sensing applications. This problem could be overcome by chemically doping graphene with heteroatoms. The doping of graphene with N and S was achieved by hydrothermally treating GO with NH_4SCN and different amount of pyrrole to obtain a sponge-like monolith graphene nanocomposite NS-G. This nanocomposites were characterized using SEM, FTIR, XPS and Raman spectroscopy. SEM images of NS-G reveals this nanocomposite to have rough curled edges due to defective sites form during heteroatoms doping. FTIR revealed functional groups on the modified material. Some peaks disappear or decrease in intensity, while other peaks appear or increase in intensity. The FTIR spectra confirm the presence of C=N, CN, and C-S bonds indicating that the doping of nitrogen and sulphur atoms has successfully entered the GO structure. XPS analysis further confirm a successful doping by displaying peaks of C, O, N, and S, and showing the atomic percentages for elemental analysis. In the Raman spectra, the I_D/I_G ratio increases with increased modification indicating disorder in the nanocomposite. The electrochemical analysis of NS-G was carried out by cyclic voltammetry and chronoamperometry. Although NS-G and GO control had the same potential window, the current peak of NS-G was way higher than the GO control. The reduction FAD and oxidation of $FADH_2$ was identified by the cathodic and anodic currents respectively. Chronoamperometry increase linearly till 2.5 mM of glucose. The NS-G could function as a glucose biosensor with linear range of 0.5 mM to 2.5 mM, a sensitivity of 6.9476 $\mu A*mM^{-1}*cm^{-2}$, and limit of detection of 0.4911 µM.

SANTRAUKA

Grafenas yra 2D vieno atomo storio sp^2 hibridizacijos būsenos anglies atomų sluoksnis, kuriame jie yra išsidėstę pagal heksagoninę simetriją. Grafenas, kaip medžiaga, pasižymi unikaliomis fizikinėmis, cheminėmis ir mechaninėmis savybėmis, lenkiančiomis kitų žinomų medžiagų charakteristikas ir įgalinančiomis panaudoti grafena pačiose įvairiausiose srityse. Deja, be šių unikalių savybių, grafenas pasižymi draustinės juostos nebuvimu, o tai sumažina jo galimybes būti pritaikytam elektrokatalizėje ir jutikliuose. Šią problemą galima spręsti, legiruojant grafeną heteroatomais. Mūsų darbe grafeną legiravome N ir S atomais, hidrotermiškai veikiant GO su NH_4SCN ir skirtingais pirolo kiekiais, susidarant kempininės konsistensijos nanokompozitiniams monolitams NS-G. Susidarę nanokompozitai buvo ištirti, naudojant SEM, FTIR, XPS ir Ramano spektroskopiją. SEM nuotraukos parodė, kad NS-G nanokompozitai pasižymi raukšlėtais kraštais, atsirandančiais legiravimo heteroatomais metu. FTIR analizė leido nustatyti nanokompozite esančias funkcines grupes. Kai kurių funkcinių grupių smailės po legiravimo sumažėja arba išnyksta, kitų – padidėja arba atsiranda. FTIR spektrai patvirtino C=N, CN ir C-S ryšių egzistavimą, tuo pačiu ir patį legiravimo sieros ir azoto atomais faktą. XPS C, O, N ir S smailių analizė taip pat patvirtino šį legiravimo faktą ir leido nustatyti nanokompozitų elementinę sudėtį. Ramano spektruose įvertinas smailių I_{D1}/I_G santykis, kuris žymi struktūrinės netvarkos padidėjimo laipsnį nanokompozituose. Susintetinti NS-G nanokompozitai buvo elektrochemiškai tirti panaudojant ciklinės voltamperometrijos ir chronoamperometrijos metodus. Nors NS-G ir GO pasižymi panašiais darbinių potencialų langais, naudojant NS-G buvo pasiektos žymiai didesnės srovės, nei naudojant kontrolinį GO. FAD redukcija ir $FADH_2$ oksidacija buvo stebėta tiriant katodines ir anodines sroves. Chronoamperometrinis atsakas didėjo tiesiškai didėjant gliukozės koncentracijai. NS-G gali būti buti panaudotas gliukozės biojutklio aktyvia medžiaga, nustatomas koncentracijų intervalas 0,5 – 2,5 mM, jautrumas – $6,6476 \mu A \cdot mM^{-1} \cdot cm^{-2}$, nustatymo minimumas – 0,4911µM.